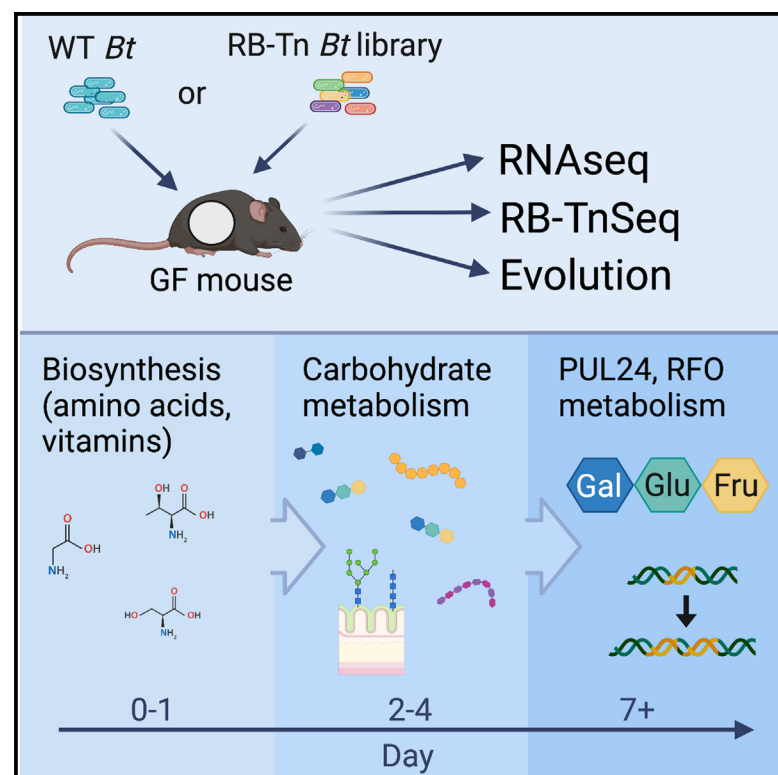


Dynamic genetic adaptation of *Bacteroides thetaiotaomicron* during murine gut colonization

Graphical abstract



Authors

Megan S. Kennedy, Manjing Zhang, Orlando DeLeon, ..., Phoebe A. Rice, Joy Bergelson, Eugene B. Chang

Correspondence

echang@medicine.bsd.uchicago.edu

In brief

Kennedy et al. evaluate temporal dynamics of *Bacteroides thetaiotaomicron* (Bt) adaptation to a new host. Bt metabolic priorities shift over the course of colonization, culminating in strong selective pressure to efficiently consume dietary resources. This work highlights the importance of considering temporal dynamics in developing better microbiome-based therapies.

Highlights

- *B. thetaiotaomicron* adaptation to the germ-free mouse gut is a dynamic process
- Early selective pressures are distinct from intermediate and long-term pressures
- Selective pressure for efficient dietary resource use dominates in the long term
- Changes in Bt spatial localization parallel changes in resource use



Kennedy et al., 2023, Cell Reports 42, 113009
August 29, 2023 © 2023 The Authors.
<https://doi.org/10.1016/j.celrep.2023.113009>

Resource

Dynamic genetic adaptation of *Bacteroides thetaiotaomicron* during murine gut colonization

Megan S. Kennedy,^{1,2,14} Manjing Zhang,^{3,14} Orlando DeLeon,⁴ Jacie Bissell,⁴ Florian Trigodet,⁴ Karen Lolans,⁴ Sara Temelkova,⁴ Katherine T. Carroll,^{4,12} Aretha Fiebig,⁵ Adam Deutschbauer,^{6,7} Ashley M. Sidebottom,⁸ Joash Lake,⁹ Chris Henry,¹⁰ Phoebe A. Rice,¹¹ Joy Bergelson,^{3,13} and Eugene B. Chang^{4,15,*}

¹Medical Scientist Training Program, Pritzker School of Medicine, The University of Chicago, Chicago, IL, USA

²Department of Ecology & Evolution, The University of Chicago, Chicago, IL, USA

³Committee on Microbiology, The University of Chicago, Chicago, IL, USA

⁴Department of Medicine, The University of Chicago, Chicago, IL, USA

⁵Department of Microbiology and Molecular Genetics, Michigan State University, East Lansing, MI, USA

⁶Environmental Genomics and Systems Biology Division, Lawrence Berkeley National Laboratory, Berkeley, CA, USA

⁷Department of Plant and Microbial Biology, University of California, Berkeley, Berkeley, CA, USA

⁸Duchossois Family Institute, Department of Biomedical Sciences, The University of Chicago, Chicago, IL, USA

⁹Committee on Immunology, The University of Chicago, Chicago, IL, USA

¹⁰Mathematics and Computer Science Division, Argonne National Laboratory, Lemont, IL, USA

¹¹Department of Biochemistry & Molecular Biology, The University of Chicago, Chicago, IL, USA

¹²Present address: Department of Chemical and Biological Engineering, Princeton University, Princeton, NJ, USA

¹³Present address: Department of Biology, Center for Genomics and Systems Biology, New York University, New York, NY, USA

¹⁴These authors contributed equally

¹⁵Lead contact

*Correspondence: echang@medicine.bsd.uchicago.edu

<https://doi.org/10.1016/j.celrep.2023.113009>

SUMMARY

To understand how a bacterium ultimately succeeds or fails in adapting to a new host, it is essential to assess the temporal dynamics of its fitness over the course of colonization. Here, we introduce a human-derived commensal organism, *Bacteroides thetaiotaomicron* (*Bt*), into the guts of germ-free mice to determine whether and how the genetic requirements for colonization shift over time. Combining a high-throughput functional genetics assay and transcriptomics, we find that gene usage changes drastically during the first days of colonization, shifting from high expression of amino acid biosynthesis genes to broad upregulation of diverse polysaccharide utilization loci. Within the first week, metabolism becomes centered around utilization of a predominant dietary oligosaccharide, and these changes are largely sustained through 6 weeks of colonization. Spontaneous mutations in wild-type *Bt* also evolve around this locus. These findings highlight the importance of considering temporal colonization dynamics in developing more effective microbiome-based therapies.

INTRODUCTION

Rapid adaptation is paramount to the survival of any species undergoing an environmental transition. For microbial taxa, which are frequently and rapidly dispersed across dramatically different habitats and microenvironments, processes of local adaptation may arise as primary determinants of microbial colonization success and resulting biogeography.¹ The mammalian gut is an environment regularly bombarded with a diverse array of exogenous microorganisms. As such, it represents a biologically and clinically relevant system to explore rapid microbial adaptational processes.

An emerging body of literature has begun probing the evolutionary and selective dynamics of exogenous microbes during

colonization of the mammalian gut but has largely neglected early-time-point or transient dynamics en route to long-term persistence. For instance, several studies using transposon sequencing (TnSeq)-based approaches have evaluated the genetic requirements for colonization across various microbes in the guts of conventionally raised, gnotobiotic, and germ-free mice, but have assessed fitness only at a single time point after introduction.^{2,3} Wu et al. evaluated TnSeq mutant abundances of four *Bacteroides* strains over a 16-day time course but performed only broad characterization of population-level shifts at intermediate time points, restricting more rigorous gene-level functional analyses to a single endpoint.⁴ Several recent evolution studies have demonstrated the extent to which carbon limitation and metabolic demands drive the evolutionary trajectories of commensal and



probiotic strains such as *Bacteroides thetaiotaomicron* (*Bt*) or *Escherichia coli* in the gut.^{5–8} However, despite dense time-course sampling, these studies do not identify genes that are important for fitness specifically at earlier stages of colonization. On shorter adaptive timescales, transcriptomics analyses of commensal microbes such as *Bt* *in vivo* and *in vitro* have demonstrated that gene expression profiles adapt quickly to factors such as diet,⁹ community membership,^{10,11} immune activation,¹² or spatial localization within the gut.¹³ However, no studies have yet comprehensively evaluated the temporal transcriptional profile of a commensal microbe over the course of colonization.

In the following experiments, we introduce a human-derived commensal organism, *Bt*, into the guts of germ-free C57Bl/6 mice to determine whether the genetic requirements for colonization shift over time and, if so, to characterize the biological functions required for microbial survival at different stages of colonization and persistence. Use of a germ-free monocolonization model allows us to reduce the staggering complexity of the gut microbial ecosystem into experimentally tractable and readily interpretable components: here, we rigorously outline population-level microbial colonization dynamics for a widely used model organism and the host-microbe interactions that drive them. Using this germ-free model as a baseline, future work can evaluate the distinct contributions of microbe-microbe interactions and other emergent community-level properties to community assembly and colonization dynamics.

To identify the microbial genes important for fitness in this context, we combine two complementary unbiased approaches: transcriptomics (RNA sequencing), which reveals global gene usage patterns, and a functional genetics approach (BarSeq^{3,14} [bar-coded anatomy resolved by sequencing]) to assess fitness consequences of gene disruptions at a global scale over the course of gut colonization. We validate these results with both *in vivo* metabolomics analysis and *in vitro* microbial growth experiments. Finally, we evaluate spontaneous evolution of wild-type (WT) *Bt* in the gut to survey natural population-level fitness dynamics. Our results indicate that adaptation to the host gut occurs in distinct stages. During the earliest stage of colonization, genes involved in amino acid and vitamin biosynthesis are upregulated and, in some cases, play essential roles in survival of *Bt*. By colonization days 2–4, *Bt* shifts toward upregulation of a diverse array of carbohydrate metabolism genes. This broad survey of available resources continues through day 7 before ultimately centering on upregulation of a polysaccharide utilization locus (PUL) responsible for the degradation of raffinose-family oligosaccharides (RFOs) rich in the standard chow diet fed to our mice. This metabolic shift accompanies a change in *Bt* localization from the mucus toward the lumen, where the expression profile remains largely consistent through at least 6 weeks of colonization. Spontaneous mutations in WT *Bt* also evolve around the same PUL, highlighting the importance of efficient carbohydrate metabolism for long-term persistence.

These experiments lay the groundwork for future delineation of shifting selective pressures in various host backgrounds and microbiome compositions. We expect that these insights into the temporally dynamic stresses that microbes must overcome to colonize and persist in the gut will prove invaluable to our understanding of microbial adaptation and the development of microbiome-based therapies.

RESULTS

Both transcriptional and genetic fitness determinants shift over the course of *Bt* colonization and persistence

To evaluate global transcription during colonization, we introduced WT *Bt* into germ-free (GF) C57Bl/6 mice and collected cecal contents at days 0.5, 1, 2, 4, 7, 14, and 42 after colonization (Figure 1A, *n* = 3–4 mice per time point). A control cohort of GF mice was gavaged with sterile phosphate-buffered saline, and *in vitro* control samples were collected from *n* = 4 *Bt* cultures at mid-log phase in brain heart infusion supplemented medium. After rRNA and host RNA depletion, the bacterial RNA samples were sequenced and compared across time points. In parallel, to assess functional genetic requirements during colonization, we introduced a rich library of randomly barcoded Tn insertion (RB-Tn) mutants of *Bt* into four different cohorts of GF C57Bl/6 mice (*n* = 3–5 mice/cohort) and collected near-daily fecal samples (Figure 1A). Amplification and sequencing of the transposon barcodes reveals the relative abundance of each mutant in the library at each time point.¹⁴ RB-Tn experiments were carried out according to two slightly different protocols, with adjustments made to optimize experimental logistics and reduce bottleneck effects (Figure S1 and STAR Methods).

First, we asked whether there are differences in *Bt* gene expression at different times after introduction into the mouse gut. We first performed principal coordinates analysis (PCoA) using Bray-Curtis dissimilarity on all gene expression data (Figure 1B). We performed PERMANOVA analysis including both experimental day and cohort as explanatory factors, and found that only experimental day significantly contributed to clustering, explaining 79% of the variation in the dataset (Table S3).

We next performed post hoc analyses to evaluate clustering by experimental day. We confirmed that the *in vitro* expression profile of *Bt* clustered distinctly from all other time points (adjusted *p* < 0.05 for all comparisons, Table S3) and excluded *in vitro* samples from further analysis. Examining *in vivo* results, we found that day 0.5 and day 1 were statistically indistinguishable, as were day 2 and day 4, and day 14 and day 42, but that all other time points formed significantly distinct clusters (Figure 1B and Table S3). Therefore, for all further analyses, day 0.5 and day 1 data were combined (“D0.5/D1”), day 2 and day 4 data were combined (“D2/D4”), and day 14 and day 42 data were combined (“D14/D42”). The largest changes in gene expression, in which samples traverse principal coordinate 1 (PC1), occurred within 2 days after introduction to the gut. Although day 7 and D14/D42 were statistically distinct, these clusters spanned a smaller and overlapping range within PCoA space, and therefore reflect relatively minor changes in global gene expression profile. To further assess overarching gene expression changes in *Bt* over 6 weeks of gut colonization, all genes that met stringent criteria of differential expression (log false discovery rate [FDR] < –3, |log₂fold change [FC]| > 2, and base mean >50 reads per million [RPM]) at any time point relative to day 1 were displayed in a heatmap (Figure 1C and Table S5). Even by these stringent criteria, we identified 489 differentially expressed genes (DEGs), which show a temporal pattern of relative peaks in expression at different time points.

Consistent with these global changes in gene expression over time, PCoA ordination using the relative abundance profiles of

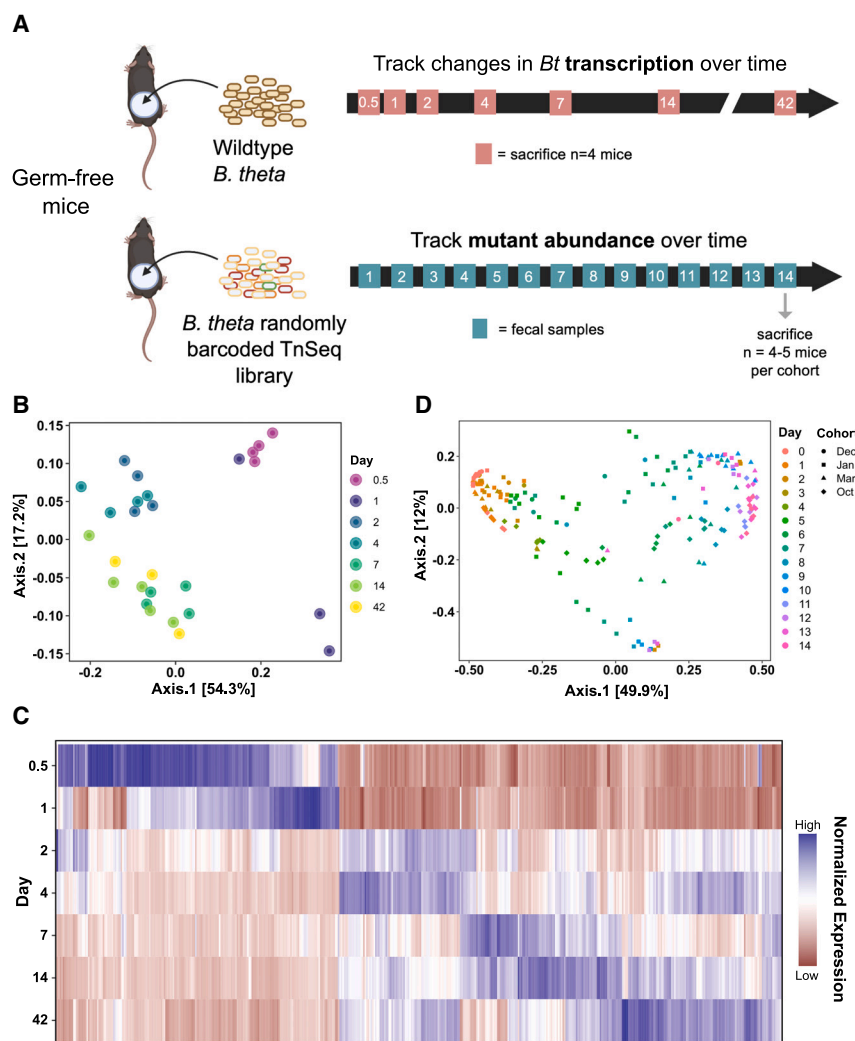


Figure 1. *Bt* gene expression and genetic fitness determinants shift over the course of colonization and persistence

(A) Experimental scheme of transcriptomics (top) and functional genetics (bottom) experiments in germ-free (GF) mice.

(B) Principal coordinates analysis (PCoA) using Bray-Curtis dissimilarity on the global gene expression profile of WT *Bt* at 0.5, 1, 2, 4, 7, 14, and 42 days of colonization (n = 4–7 per group).

(C) Heatmap visualizing all genes that were significantly differentially expressed at any time point relative to day 1 (criteria: $\log_{10}FDR < -3$, $|\log_2FC| > 2$, base mean >50 RPM). Each column represents an individual gene (Table S5); data are normalized across all time points for each gene.

(D) PCoA using Bray-Curtis dissimilarity on the abundances of RB-Tn mutant strains in fecal samples, colored by experimental day, shaped by experimental cohort. Four different cohorts of mice (n = 3–5 per cohort) are represented.

See also Tables S3 and S5.

the RB-Tn mutant strains within each mouse in our functional genetics experiment reveals that the mutant pool composition shifted across time in a replicable pattern (Figure 1D) across four independent cohorts of this experiment (Figure 1D) protocol adjustments. PERMANOVA showed that the data cluster significantly by experimental day ($p = 0.0001$, $R^2 = 0.457$), with less substantial but significant contributions by individual mouse ID ($p = 0.0001$, $R^2 = 0.135$) and experimental cohort ($p = 0.0001$, $R^2 = 0.092$). The largest shifts across PC1 occurred between day 1 and day 7, with the mutant pool changing less dramatically between day 7 and day 14. Together, these data suggest that different sets of genes mediate colonization and growth immediately upon gut entry and later in the adaptational process.

Amino acid and vitamin biosynthesis are transcriptionally upregulated and functionally significant during early colonization of the gut

To gain a more comprehensive understanding of the gene pathways expressed during the acute phase of adaptation to the gut, we performed pairwise comparisons of gene expression across sequential time points. We identified extensive shifts in the *Bt* tran-

scriptome between D0.5/D1 and D2/D4, with expression of 85 genes relatively enriched on D0.5/D1 and expression of 192 genes enriched at D2/D4 (Figure 2A). The pathways enriched at D0.5/D1 comprised a largely unique set of genes from those that dominate the *Bt* expression profile *in vitro* (Table S5). To functionally characterize these DEGs, we mapped them to the Kyoto Encyclopedia of Genes and Genomes (KEGG) catalog (Figure 2B). Although fewer DEGs were upregulated at D0.5/D1 compared to D2/D4, more of these genes mapped to known KEGG pathways, spanning a variety of functions, many of which center around

metabolism. In particular, 30 DEGs upregulated at D0.5/D1 mapped to amino acid metabolism functions compared to ten amino acid genes upregulated at D2/D4.

To further explore the metabolic functions characteristic of the early phase of colonization, we performed gene set enrichment analysis (GSEA) for all KEGG metabolism modules across D0.5/D1 and D2/D4 (Figure 2D). Expression of pathways corresponding to the biosynthesis of many amino acids was enriched specifically at the D0.5/D1 time point. Expression of genes involved in the biosynthesis of biotin, a cofactor required for amino acid biosynthesis, was concurrently upregulated at D0.5/D1. These results are supported by RB-TnSeq analysis: by mapping the significantly depleted gene mutants (t statistic $< -3\sigma$) on the first day of the functional genetics assay using KEGG, we identified amino acid metabolism as the KEGG family with the largest number of significantly depleted mutants (Figure 2C). These genes are identified by gold stars on the amino acid biosynthesis pathway map in Figure S2, which illustrates reactions with upregulated gene expression at D0.5/D1 compared to D2/D4. We observe that biosynthesis of most amino acids involves multiple reactions that are transcriptionally enriched at D0.5/D1, or one step that is functionally essential.

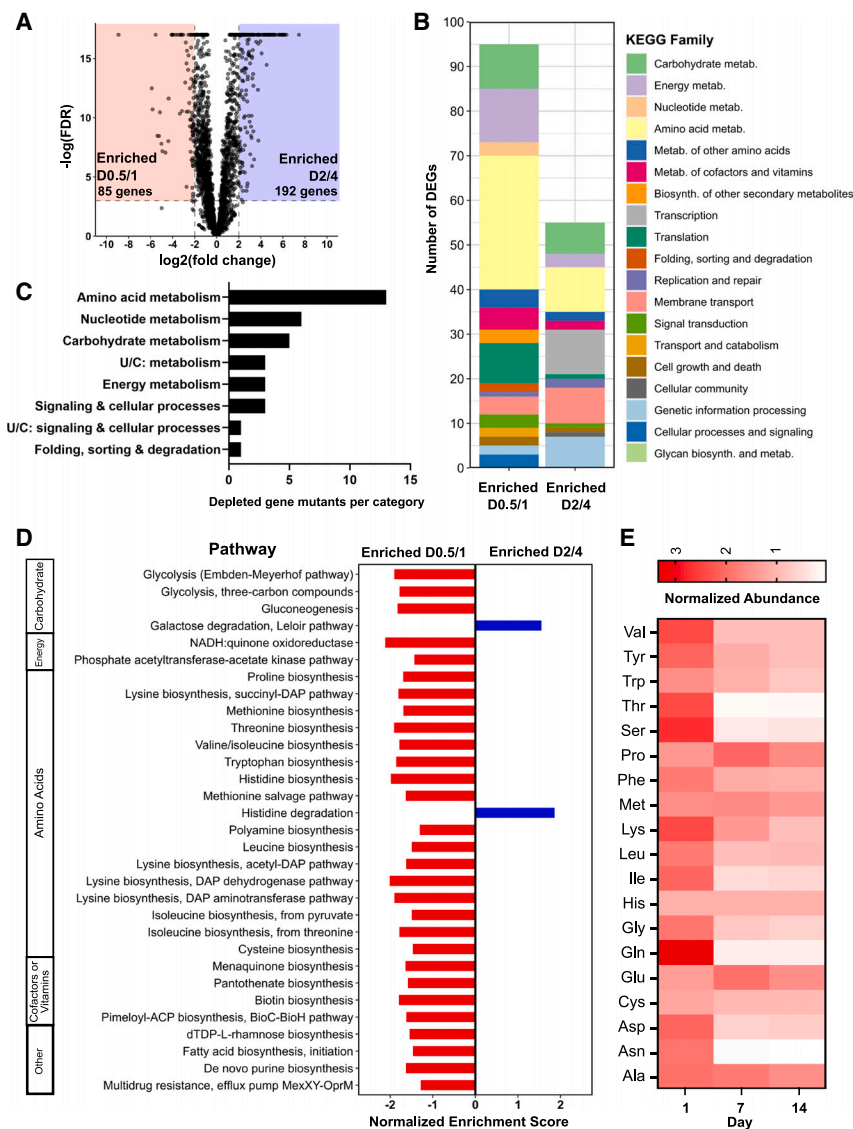


Figure 2. The *Bt* transcriptome undergoes dramatic remodeling during the first week after introduction to the murine gut

(A) Volcano plot of significant transcriptional differences between day 0.5 (D0.5/D1) and D2/D4. Eighty-five genes had significantly increased expression on D0.5/D1 (red), while 192 had significantly increased expression on D2/D4 (blue) (cutoff: $\log(\text{FDR-adjusted } p \text{ value}) < -3$, $|\log_2\text{FC}| > 2$, maximum group mean >50 RPM).

(B) DEGs from (A) colored by KEGG family. Genes with no KEGG annotations were excluded.

(C) Number of gene mutants significantly depleted in the RB-Tn experiment (t statistic $< -3\sigma$) on day 1 of the experiment, plotted by KEGG family.

(D) GSEA using transcriptomics data for all KEGG metabolic modules, comparing D0.5/D1 to D2/D4. Only pathways with significant differential expression ($p < 0.05$) are shown.

(E) Abundances of amino acids in the ceca of ex-GF mice at day 1, day 7, and day 14 of colonization measured using gas chromatography-mass spectrometry (GCMS) and normalized to internal standards and to respective GF day-0 controls ($n = 5$ mice for GF day 0, $n = 4$ for post-colonization samples). See also Table S5.

Not only do both our transcriptomics analysis and functional genetics screen support a key role for amino acid biosynthesis early in colonization, but metabolomic analysis of the cecal contents corroborates this finding. We measured the levels of specific amino acids in the cecum of GF mice and compared those to cecal levels in ex-GF mice at day 1, day 7, and day 14 after colonization with WT *Bt*, and found that amino acid levels were generally higher on day 1 than on day 7 or day 14 (Figure 2E), as shown previously in an *E. coli* colonization model.⁸ This difference was especially profound and statistically significant for amino acids in the glycine-serine-threonine pathway and for asparagine (Table S4). By contrast, glutamate and proline reach their highest levels at day 7 before being depleted in the second week.

Although upregulation of amino acid and vitamin biosynthesis at D0.5/D1 is reminiscent of the stringent response (SR), in which growth is inhibited under conditions of nutrient limitation to prioritize biosynthesis of essential nutrients,¹⁵ further analysis suggests that early colonization is a distinct transcriptional program. Using a

zation, these likely represent a distinct but overlapping response to the shifting selective pressures of the gut resource environment.

A shift toward enhanced expression of diverse sugar metabolism genes occurs during the first week of gut colonization

Of the 192 DEGs upregulated at D2/D4 compared to D0.5/D1, only 50 mapped to known KEGG orthologs (Figure 2B and Table S5). Among these, we noted specific enrichment of genes involved in transcription, membrane transport, and genetic information processing, which represents *Bt*'s seven identical insertion sequence 3 (IS3)-family transposases. In the functional genetics experiment, we found that by day 2, amino acid metabolism had been surpassed by carbohydrate metabolism as the KEGG family with the largest number of depleted gene mutants (Figure 3A). This suggests that amino acid metabolism becomes less functionally essential after day 1 and that efficient carbohydrate metabolism becomes more essential.

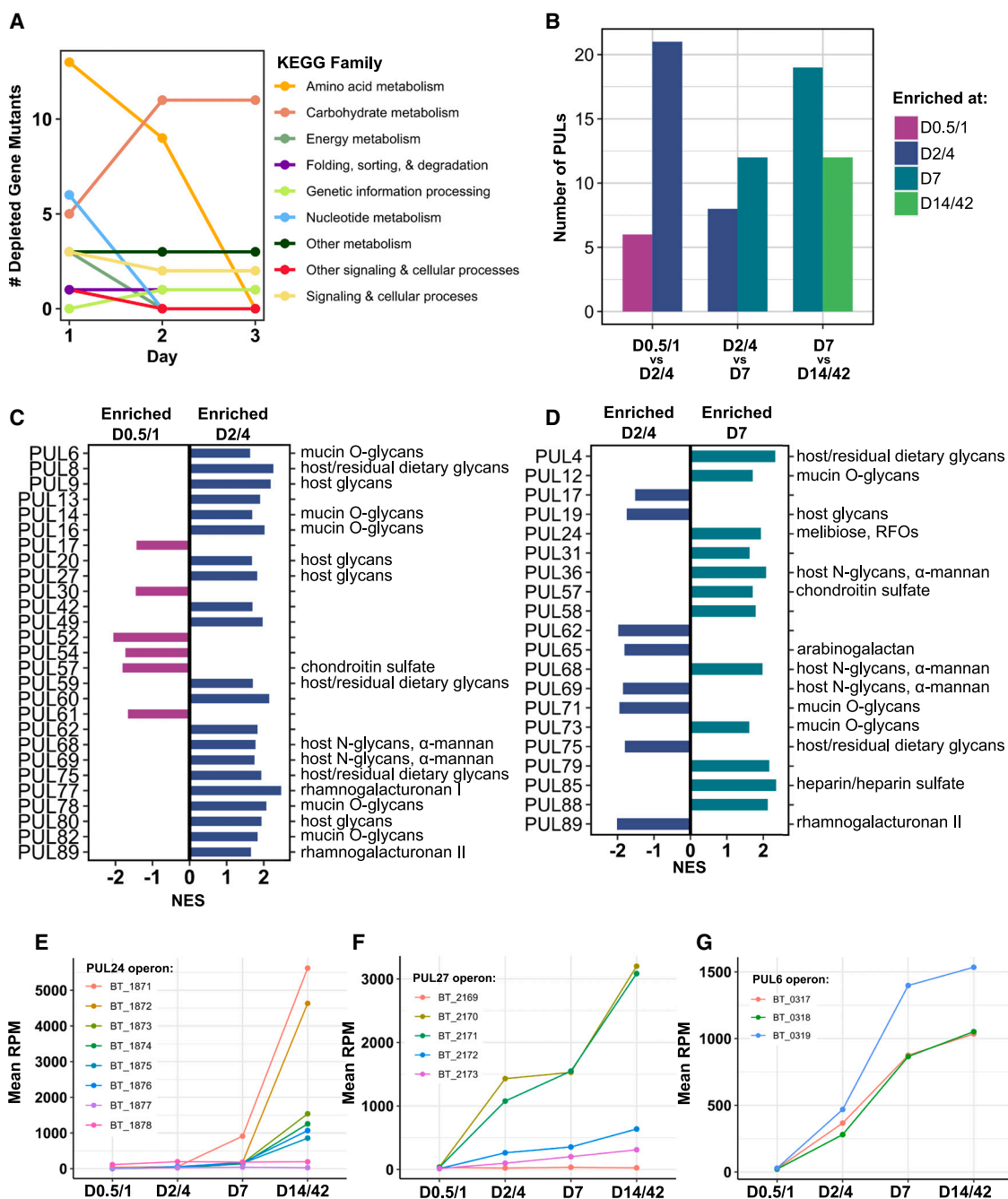


Figure 3. A shift toward greater expression of diverse sugar metabolism genes occurs during the first week of gut colonization

(A) Number of gene mutants significantly depleted from day 1 to day 3 of the RB-Tn experiment (t statistic $< -3\sigma$), colored by KEGG family.

(B–G) Number of PULs significantly differentially expressed (adjusted $p < 0.05$) across sequential pairwise comparisons identified via GSEA using transcriptomics data. Specific PULs differentially expressed across (C) day 0.5 (D0.5/D1 vs. D2/D4) and (D) D2/D4 vs. D7 identified via GSEA. Predicted PUL substrates are listed on the right. Mean expression levels (RPM) for all genes in the (E) PUL24, (F) PUL27, and (G) PUL6 operons. Error bars excluded for visual clarity; statistical comparisons done via GSEA. See also Table S5.

Members of the genus *Bacteroides* are well known for their ability to digest a wide variety of polysaccharides.^{17–19} According to the CAZy database, *Bt* possesses 359 glycoside hydrolases, 87 glycosyl transferases, 15 polysaccharide lyases, and 19 carbohydrate esterases.²⁰ To further probe carbohydrate utilization, we

performed GSEA on all PULs in the *Bt* genome in pairwise comparisons across sequential time points. Across all time points, 49 unique PULs were significantly differentially expressed. We find that from D0.5/D1 to D2/D4, expression of 21 PULs was upregulated compared to only six that were downregulated (Figures 3B

and 3C). From D2/D4 to day 7, 12 PULs were upregulated compared to eight that were downregulated (Figures 3B and 3D), and from day 7 to D14/D42, more PULs were downregulated than upregulated (Figure 3B). Collectively, these data show that over the first week of colonization, *Bt* increases expression of a broad array of PULs, but expression of many of these PULs is reduced as time goes on, perhaps to optimize utilization of available resources.

To identify specific PULs that may be particularly central to efficient resource utilization, we searched for PUL genes whose mean expression across mice increased monotonically over all time points, and found genes belonging to 21 PULs, including PUL24 and PUL59, both of which are adjacent to IS3-family transposases (Table S5). Of these 21 PULs, only PUL24, PUL27, and PUL6 had expression patterns that were broadly consistent across all genes in the PUL (Figures 3E and 3F). These PULs moreover reached substantially higher levels of expression (~1,500–6,000 RPM) than any of the other 18 PULs (~200–400 RPM). PUL27 and PUL6 are predicted to enable degradation of host mucosal glycans, suggesting that *Bt* may be foraging for sugars through degradation of the mucus layer.¹⁷ The last gene of PUL24 encodes an α -galactosidase (BT1871), which is predicted to confer the ability to hydrolyze the α -1,6 glycosidic linkage in RFOs, a major component of the fiber-rich diet fed to our mice, as well as many standard mouse chows.⁵ Although this study focuses on understanding the shifting genetic determinants of colonization over time, we recognize that the effect of diet is intrinsic to the results of any gut microbiome study.

Global *Bt* gene expression stabilizes after 1 week of colonization

In contrast to the 277 DEGs identified between D0.5/D1 and D2/D4, we found only 21 DEGs that met our criteria between D2/D4 and day 7, and only seven between day 7 and D14/D42 (Table S5). Of the DEGs between D2/D4 and day 7, the only one that mapped to any KEGG pathway was in the PUL24 operon, and similarly, five of the seven DEGs between day 7 and D14/D42 fell into the PUL24 operon. Thus, we infer that *Bt*'s transcriptional profile has largely stabilized within the first week of colonization and is maintained thereafter, excepting the continued upregulation of certain PUL genes.

Upregulation of α -galactosidase activity confers a significant growth advantage to *Bt* in GF mice fed a standard RFO-rich diet

Our functional genetics screen confirmed the importance of PUL24: around 4 days after introduction of the RB-Tn mutant library into GF mice, the diversity of the community begins to collapse due to strong positive selection for a small pool of mutants that seemed to have gained fitness from the Tn insertion (Figure 4A). This could be caused by RB-Tn insertions in regulatory elements or by polar effects on downstream genes driven by readthrough from the antibiotic resistance promoter of the RB-Tn insertion.³ RB-Tn mutants with insertions in PUL24 were among the most positively selected mutants at the end of the 2-week experiment, exhibiting growth that exceeded a neutral expectation that final abundances would simply reflect initial

abundances in the inoculum (Figure 4B). Furthermore, most of the hyperfit mutants had Tn insertions in one of three operons: PUL24 (BT1871–1877), PUL39 (BT2851–2860), or BT3130–3134, all of which encode at least one α -galactosidase, situated at the tail end of the operon (Figure 4C). At the end of the RB-Tn selection experiments, the populations were overtaken by mutants carrying Tn insertions upstream of these α -galactosidase genes (Figure 4D). This was true for all mice across four independent experimental cohorts, which were carried out months apart from one another (Figure 4E).

This RB-Tn pool has previously been assayed in over 300 different conditions including distinct carbon or nitrogen sources and specific stress conditions.³ The mutants that we identified as hyperfit in GF mice exhibit a phenotype significantly deviant from WT in only two conditions: within GF mice and in defined culture with melibiose—a disaccharide of glucose and galactose, and a breakdown product of the trisaccharide raffinose (Figure S3A)—as the sole carbon source. In both cases, these mutants exhibit a growth advantage. Indeed, when we isolated the most abundant strains from day 14 of the RB-Tn experiment, we found that their growth rate was significantly higher than WT when melibiose is the sole carbon source (Figure 5A and Table S6). In this condition, *Bt* must hydrolyze the α -1,6 glycosidic bond to harvest and metabolize the monosaccharide sugars. The competitive advantage of these mutants cannot be attributed to either of the monosaccharides or to hydrolysis of α -1,2 glycosidic bonds, as the mutant growth rates on these carbon substrates (glucose, galactose, and sucrose) are indistinguishable from WT (Figure S3B). In raffinose medium, which contains both α -1,2 and α -1,6 linkages, mutants exhibit an attenuated but still significant growth advantage (Figure S3B, $p = 3.9 \times 10^{-5}$, t test, $n = 4$ –6).

Given that release of the monosaccharide sugars of melibiose depends on hydrolysis of an α -1,6 glycosidic bond, we hypothesized that the fitness phenotypes both in mice and *in vitro* did in fact depend on overexpression of the α -galactosidase gene downstream of the Tn insertion site. To test the hypothesis that the Tn insertion enhanced expression of downstream genes, we grew WT and hyperfit mutants in melibiose medium and measured the expression of α -galactosidase genes. For this experiment we used two mutants, one carrying an insertion in PUL24 and another carrying an insertion in the BT3130–3134 operon. For both mutants, we found >10-fold overexpression of α -galactosidase downstream of the insertion but within the same operon (Figure 5B, BT1871: $p < 1 \times 10^{-6}$, t test; BT3131: $p = 4 \times 10^{-6}$, $n = 3$ –4/group). Meanwhile, expression of an α -galactosidase (BT2851) located outside the operons that carry the insertion was similar between WT and the mutants.

We then overexpressed BT1871 from a strong, constitutively active promoter (P_{rpoD}) in WT *Bt* and observed a 3-fold increase in log-phase growth rate relative to WT when melibiose was the sole carbon source (Figure 5A and Table S6). We note that even this constitutive-expression mutant did not exhibit as much growth advantage as the RB-Tn mutant strains. It is possible that the RB-Tn strains may have evolved additional mutations that further promote growth on melibiose media, although we identified no new junctions suggesting genomic rearrangements

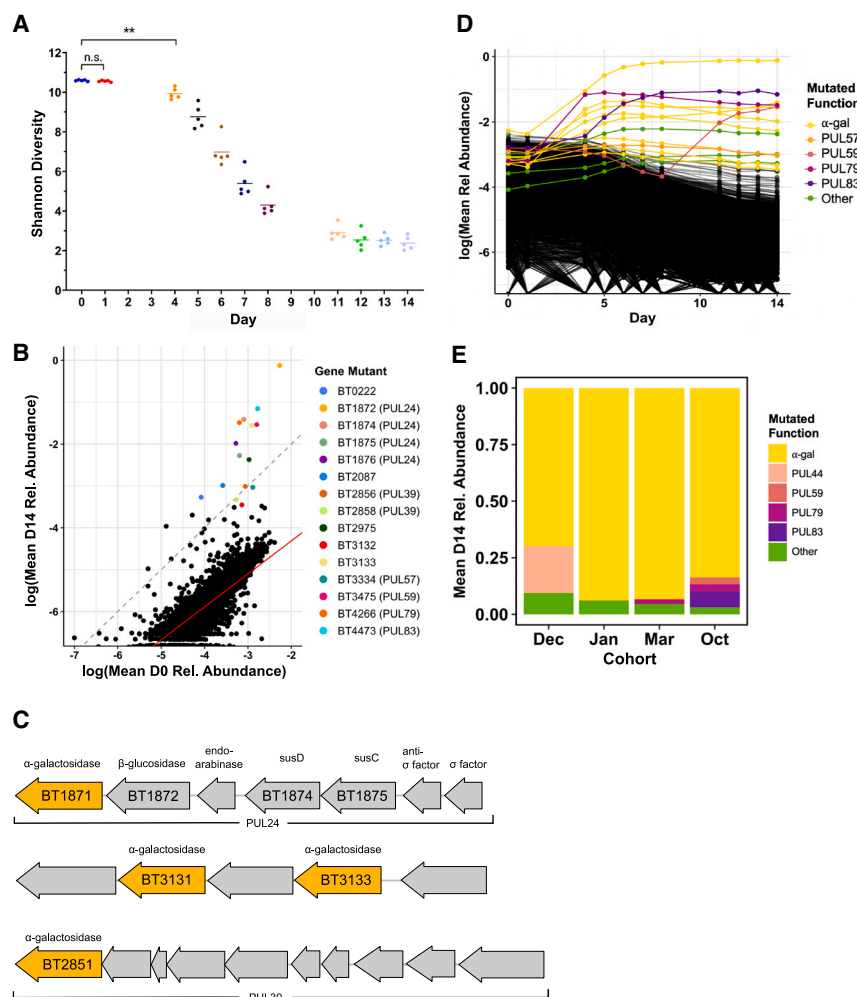


Figure 4. Colonization of a complex *Bt* mutant library within GF mice selects for disruptions upstream of α -galactosidase genes A–D) (A, B, and D) Data from a single experimental run (October). (A) Shannon diversity of the RB-Tn mutant pool in mice over time. Each point represents the RB-Tn pool within a single mouse on the indicated day ($p < 0.01$, t test, $n = 5$ /time point). (B) Initial (inoculum, day 0) vs. final (day 14) relative abundance of RB-Tn mutant strains. Each point represents the summed relative abundance of all mutant strains that mapped to given gene, averaged across mice. Dashed gray line designates a 1:1 relationship between starting and final abundance; red line represents a linear regression best-fit line generated from the log-transformed data ($p < 2e-16$, $R^2 = 0.6461$; STAR Methods). (C) Organization of PUL 24 (BT1871–1877), an unnamed PUL containing BT3130–3134, and PUL 39 (BT2851–2860). Predicted α -galactosidases are colored yellow. (D) Relative abundance of RB-Tn mutant strains over time. Each line represents the summed relative abundance of all mutant strains that mapped to a given gene, averaged across mice. Top 15 most abundant gene mutants at day 14 are colored by the PUL to which they mapped; all others are black. (E) Day-14 relative abundance of gene mutants mapping to operons that encode α -galactosidase functions (yellow), known PULs, or other gene functions averaged across mice for each experimental run.**

and no changes in coverage suggesting duplications in whole-genome short-read sequencing of RB-Tn isolates. Alternatively, the promoter used in front of the erythromycin resistance cassette in the RB-Tn mutants may simply be stronger than the P_{rpoD} promoter we used here.

Metabolomic measurements of a carbohydrate panel confirm that raffinose and its constituent sugars are among the most abundant carbohydrate substrates within the ceca of GF mice fed a standard chow (Figure 5C). Although mammals can catalyze hydrolysis at the α -1,2 linkages in raffinose and sucrose, the α -1,6 linkages in raffinose and melibiose can only be hydrolyzed by gut microbes (Figure S3A).²² Accordingly, raffinose and melibiose build up in the cecum of our GF mice at high concentrations until *Bt* is introduced. After 7 days, during which time *Bt* has initiated overexpression of α -galactosidase genes, these sugars are depleted (Figure 5D, $p = 0.02857$, Wilcoxon test, $n = 4$; Figure S3C, $p = 0.006193$, t test, $n = 4$). In contrast, sucrose is consumed by the host and no significant changes are observed in sucrose concentration following *Bt* colonization (Figure S3D).

Together, we find that when mice are fed standard high-fiber chow, the high concentration of RFOs accumulating in the

lower gastrointestinal (GI) tract creates an environment that strongly selects for *Bt* strains that can make efficient use of these sugars through increased expression of α -galactosidases. We infer that efficient carbohydrate metabolism—particularly for abundant dietary fibers—is a major determinant of population-level selective dynamics during the persistence phase of *Bt* engraftment within the gut.

Changes in resource-use strategies coincide with shifts in *Bt* localization from the mucus toward the lumen

We next sought to determine whether *Bt* localization changes over the course of colonization. To assess *Bt* localization at days 1, 2, 4, 7, and 42, we labeled fixed colonic cross-sections with antibodies to MUC2, the predominant colonic mucin,²³ and the DNA stain 4',6-diamidino-2-phenylindole (DAPI), and imaged them with a laser-scanning confocal microscope. We then quantified the average epithelial proximity of *Bt* by measuring the distance from the epithelial surface along perpendicular tracts to the nearest bacterial cell (STAR Methods).

At days 1 and 2, *Bt* was deeply embedded within a largely unstructured mucus layer, often directly adjacent to the epithelium (Figures 6A and 6B). By day 4, an observable but thin and patchy inner mucus layer began to form (Figure 6C), which expanded in thickness by day 7 (Figure 6D). This layer still allowed substantial penetration by *Bt*, although mean distance from *Bt* to the epithelium was significantly increased compared

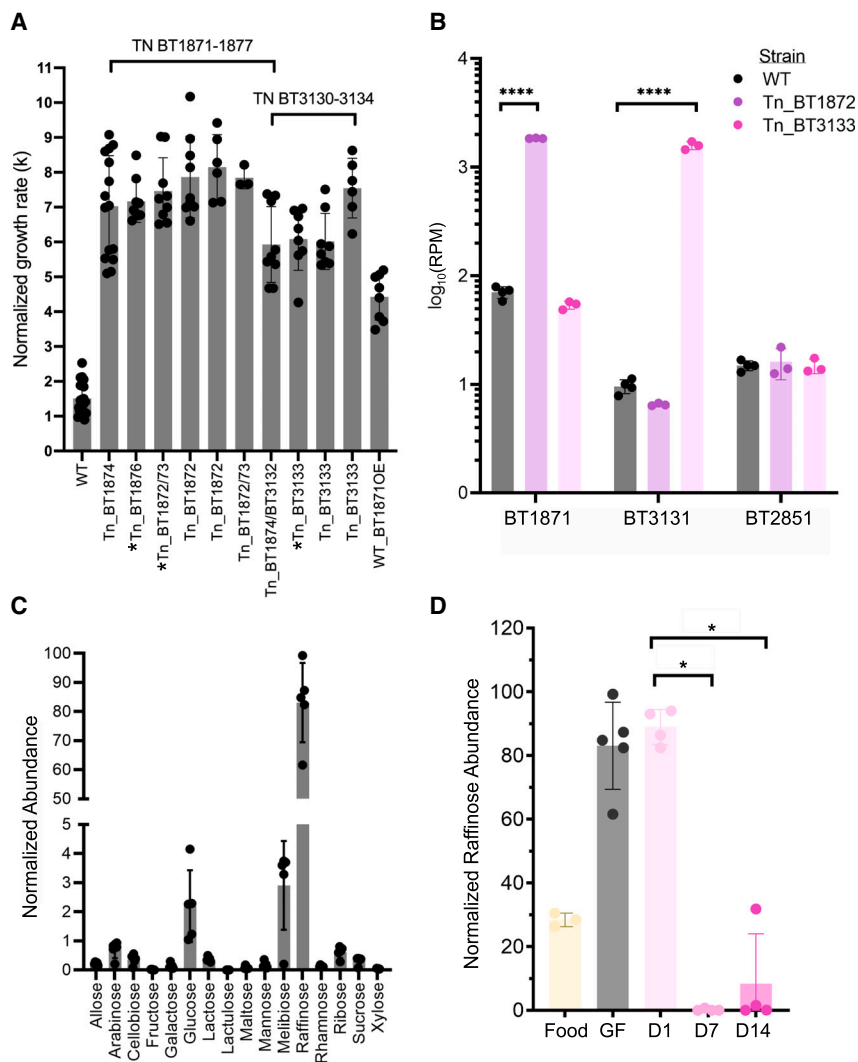


Figure 5. Upregulation of α -galactosidase activity confers a significant growth advantage to *Bt* in GF mice fed a standard RFO-rich diet

(A) Log-phase growth rates (k) of the most abundant RB-Tn mutant strains isolated from mice and grown in melibiose minimal medium. Strains with asterisks carry other mutations in addition to the transposon insertion. The WT + BT1871OE strain carries a plasmid copy of BT1871 expressed from the *rpoD* promoter that was integrated into the WT genome at the attN1 site. All mutant strains grew significantly faster than WT ($p < 0.0001$).

(B) Normalized abundance of α -galactosidase mRNA (RPM) measured in WT and hyperfit RB-Tn mutants isolated from mice and grown in Varel-Bryant defined medium with 20 mM melibiose as the sole carbon substrate.²¹

(C) Abundance of various sugars in the GF mouse cecum as measured using GCMS and normalized to internal standards.

(D) Abundance of raffinose in the standard chow fed to GF mice, within GF ceca before colonization, or 1, 7, or 14 days post colonization.

* $p < 0.05$; ** $p < 0.01$; *** $p < 0.0001$, **** $p < 0.00001$. See also Table S6.

Strong selection for efficient RFO metabolism leads to emergence of spontaneous *Bt* mutants with duplicates of the BT1871 locus through an IS3-family transposable element

The transposon mutants in our functional genetics experiment were able to gain ~ 10 -fold increase in α -galactosidase expression due to readthrough from an extremely strong, synthetic promoter. We wondered whether the selective pressure for elevated α -galactosidase activity to uti-

lize the α -1,6-linked sugars abundant in the diet would drive evolution of a spontaneous mutant with enhanced α -galactosidase activity. One week after the initial colonization of GF mice with WT *Bt* in an ongoing transcriptomics experiment, three mice from two cages were separated into individual cages for 6 weeks of observation, a length of time predicted to be sufficient for spontaneous mutations to arise and stabilize.⁷ At the end of 6 weeks, we performed shotgun sequencing on fecal material from all three mice. Assembly of the short-read sequences revealed that there was at least 2 \times coverage of the BT1871 locus for all samples (Figure 7A). A dip to 1 \times coverage in the middle of this region mapped to an IS3-family transposase, of which there are six other identical copies in the genome; hence, the corresponding coverage was diluted among the different copies. BreSeq analysis identified three new junctions in the *Bt* genome indicative of genome rearrangements (Figure 7B). Notably, samples from mouse A and mouse C, which were co-housed during the first week of the experiment, shared an identical junction, suggesting that this mutation arose in *Bt* within the first week

to day 1 (Figure 6F, $p = 0.037$, t test, $n = 4$ /group). At day 42, a defined inner mucus layer covered the epithelial surface of each cross-section, effectively excluding *Bt*, which localized primarily to the shedding outer mucus layer and luminal space (Figures 6E and 6F, $p = 0.024$, t test, $n = 3$ –4/group). Thus, as the impermeable mucus layer forms, we identify a shift in *Bt* spatial localization from deeply embedded in the mucus layer early in colonization toward the luminal space by day 7 and onward.

Our RNA-sequencing data indicated that *Bt* undergoes a metabolic shift around day 7 of colonization, switching from broadly upregulated PUL metabolism, including many loci predicted to encode mucosal glycans, to a metabolic profile strongly centered around dietary RFO consumption. Here, we find that *Bt* spatial localization similarly shifts around day 7 of colonization from the mucus into the lumen. We have therefore identified a loose correlation between the timing of shifts in *Bt* resource-use strategies and its spatial localization with respect to the mucus layer and luminal space.

lize the α -1,6-linked sugars abundant in the diet would drive evolution of a spontaneous mutant with enhanced α -galactosidase activity. One week after the initial colonization of GF mice with WT *Bt* in an ongoing transcriptomics experiment, three mice from two cages were separated into individual cages for 6 weeks of observation, a length of time predicted to be sufficient for spontaneous mutations to arise and stabilize.⁷ At the end of 6 weeks, we performed shotgun sequencing on fecal material from all three mice. Assembly of the short-read sequences revealed that there was at least 2 \times coverage of the BT1871 locus for all samples (Figure 7A). A dip to 1 \times coverage in the middle of this region mapped to an IS3-family transposase, of which there are six other identical copies in the genome; hence, the corresponding coverage was diluted among the different copies. BreSeq analysis identified three new junctions in the *Bt* genome indicative of genome rearrangements (Figure 7B). Notably, samples from mouse A and mouse C, which were co-housed during the first week of the experiment, shared an identical junction, suggesting that this mutation arose in *Bt* within the first week

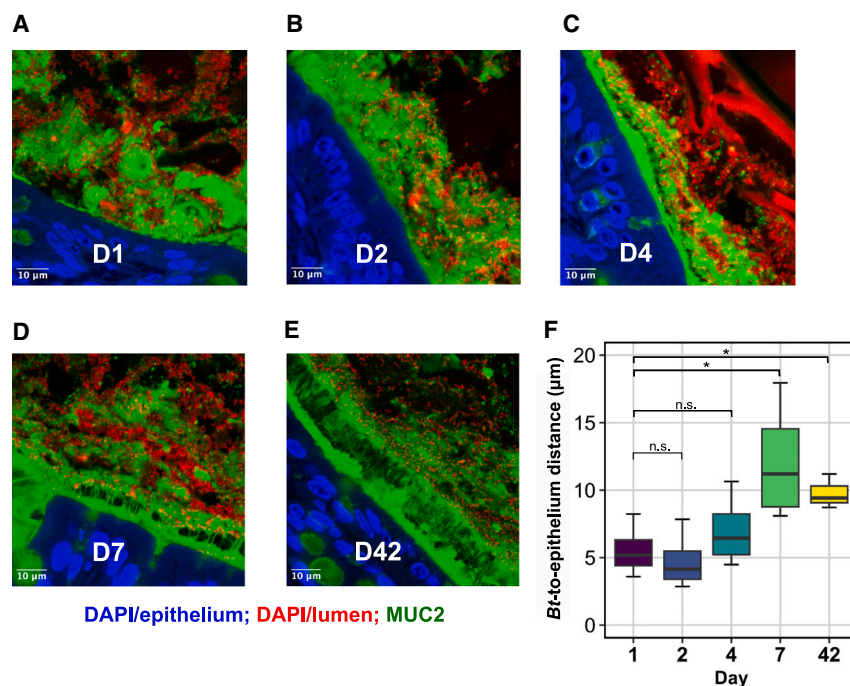


Figure 6. *Bt* localization shifts from the mucus toward the luminal space over colonization

(A–E) Representative cross-sections of distal mouse colon fixed in Carnoy's solution at (A) day 1 (D1), (B) D2, (C) D4, (D) D7, and (E) D42 of colonization by *Bt*. Blue, DAPI staining in the epithelium; red, DAPI staining in the lumen of gut, including bacteria, debris, and shed host nuclei; green, antibody staining for MUC2. Scale bars, 10 μm.

(F) Mean *Bt* epithelial proximity. $n = 3$ –4/group, t test, $*p < 0.05$.

of colonization and was transmitted across mice. Samples from mouse B and mouse C each possessed unique junctions, indicating that these junctions arose independently. In all, three independent junctions spontaneously evolved in this experiment, and all three junctions were formed between either BT1872 or BT1873 and a locus downstream of BT1871, which encodes for rRNAs, tRNAs, and a ribosome recycling factor. All three new junctions occupied a significant portion of the sequencing reads (60%–73%), suggesting that the mutants carrying these junctions were competitively dominant in the gut environment.

IS3-family transposases are known to act by a copy-and-paste mechanism.²⁴ We wondered whether this transposase, which we had identified as significantly upregulated from D0.5/D1 to D2/D4 (Table S5), could have created multiple copies of the BT1871 locus. We isolated individual strains likely to contain these mutations by plating bulk fecal material and then selecting a single strain from each mouse that exhibited a growth advantage compared to WT on melibiose medium (Figure 7C). We then performed long-read sequencing of each strain with MinION. In one of these isolates, we identified a tandem repeat of the BT1871 locus (Figure 7D), which places the original copy of BT1871 downstream of a strong rRNA promoter. Interestingly, the six identical copies of this IS3-family transposase (NCBI: 60924995) are often found adjacent to PULs in the WT *Bt* genome. This suggests that these transposable elements confer a mechanism to modulate gene expression that may be advantageous in adapting to new metabolic landscapes.

Interactions with the host are relatively consistent throughout colonization

Although the host response to monocolonization is not the focus of this paper and has been thoroughly cataloged elsewhere,^{25–28} we assessed levels of cecal immunoglobulin A (IgA) and serum IgG, as

well as several pro-inflammatory cytokines from colonic mucosal scrapings. We identified no significant or consistent trends in any of these metrics (Figure S4). Previous work has outlined how IgA binding to commensal bacteria such as *Bt* may impact gene expression, in some cases affecting dietary polysaccharide usage and microbial localization.^{27,29–31} We could not recapitulate these specific changes in our *Bt* gene expression time course. This may reflect differences in IgA assay protocols,²⁹ or it may suggest that *Bt*'s response to IgA binding is sensitive to the specific mouse chow composition and availability of dietary resources.

We then performed targeted GSEA on expression of *Bt*'s capsular polysaccharide (CPS) loci, which encode outer membrane proteins that mediate interaction between *Bacteroides* genera and the host immune system³² and have been shown previously to play a critical role in *Bacteroides* gut colonization.^{2,33,34} We found that CPS loci 1 and 3, and to a lesser extent 2, 4, and 7, were highly expressed early in colonization and then downregulated, whereas CPS5 and CPS6 had increasing relative expression from day 7 onward (Figures S5A–S5D). Only CPS4 mutants showed severe fitness defects during the early days of the functional genetics assay, in line with previous reports (Figure S5E).² These data indicate that *Bt* modifies its outer membrane upon entry into the gut and over the course of persistence, which may reflect adaptation to the host immune system, perhaps in parallel to shifts in localization.

well as several pro-inflammatory cytokines from colonic mucosal scrapings. We identified no significant or consistent trends in any of these metrics (Figure S4). Previous work has outlined how IgA binding to commensal bacteria such as *Bt* may impact gene expression, in some cases affecting dietary polysaccharide usage and microbial localization.^{27,29–31} We could not recapitulate these specific changes in our *Bt* gene expression time course. This may reflect differences in IgA assay protocols,²⁹ or it may suggest that *Bt*'s response to IgA binding is sensitive to the specific mouse chow composition and availability of dietary resources.

DISCUSSION

Microbial adaptation during colonization is a dynamic process

Bacteroides species are dominant and prevalent in the guts of many human populations.^{35,36} Instrumental to their success is their ability not only to tolerate stress but to quickly adapt in order to grow under a range of conditions.^{37,38} Although *Bt* has been used as a model organism to understand the genetic drivers of gut colonization for commensal organisms,^{2,4,39} a single representative time point has been assessed in most previous investigations, which fail to consider the dynamism of the adaptational process. For example, whereas previous work based on *in vivo* *Bt* gene expression at a single time point characterized only

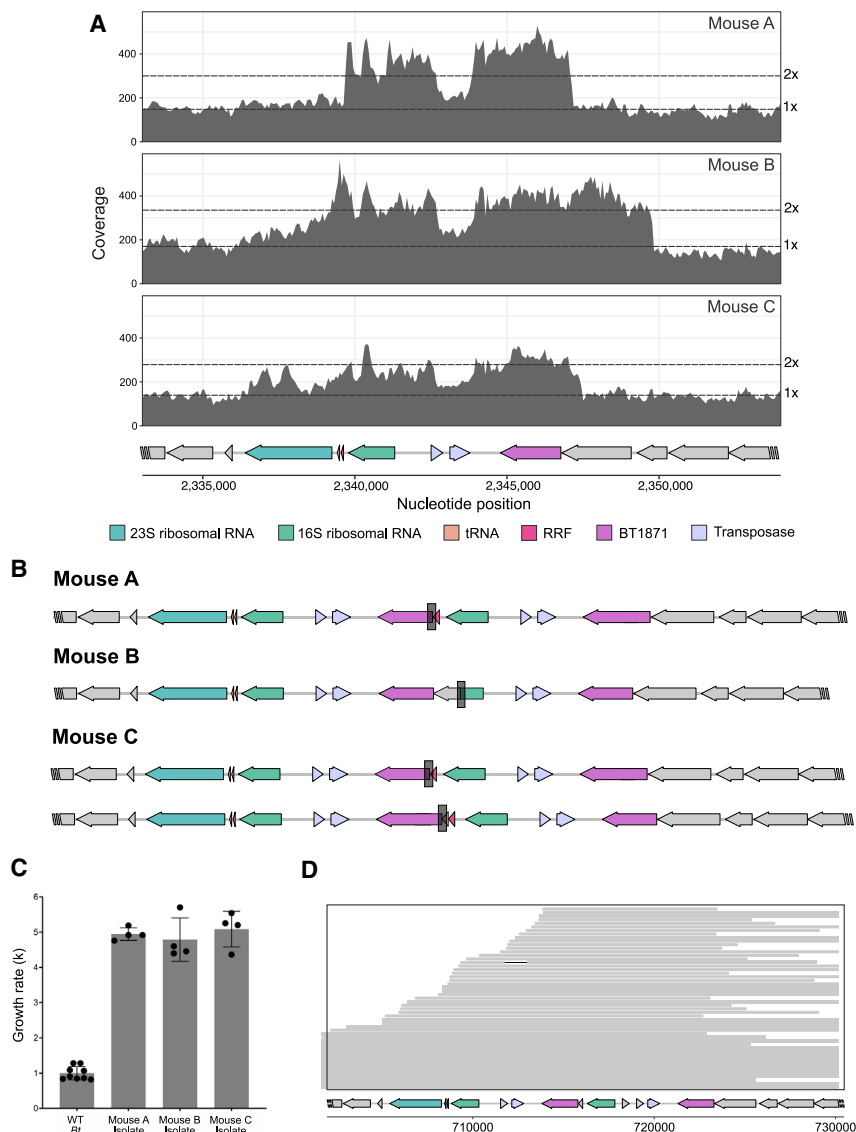


Figure 7. Under strong selective pressure, *Bt* duplicates the BT1871 locus with the help of a transposable element

(A) Shotgun sequencing of bulk fecal sample from three mice inoculated with WT *Bt* shows at least 2x coverage of the BT1871 locus.

(B) New *Bt* genomic junctions identified via shotgun sequencing of bulk fecal material from each mouse. (C) Log-phase growth rates (k) of three mutant strains isolated from feces of mice colonized with WT *Bt* for 6 weeks compared to growth rate of the ancestral WT *Bt* in defined medium supplemented with melibiose ($n = 4$ technical replicates per strain). $p < 0.05$.

(D) Long-read MinION sequencing of an abundant mutant in mouse C (MZ65) reveals the duplication of a long segment including the BT1871 gene, which generates a tandem repeat of the locus. Each gray bar represents a single long read, which together span the region containing the tandem repeat.

Early colonization is a distinct adaptational phase

The process of colonizing a new host presents a diverse array of environmental changes that require physiological adaptation. The largest transcriptomic changes that we observed across 6 weeks of *Bt* colonization occurred in the first week (Figure 1B), as did the largest shifts in RB-Tn mutant abundances (Figure 1C). Our findings indicate that *Bt* upregulates a broad swath of metabolic processes upon arrival in the lower GI tract during the earliest stage of colonization (Figure 2B). Work from Watson et al. examining the qualities of microbes that successfully colonize the gut after fecal microbial transplant suggests that microbes that can be metabolically “self-sufficient” may be better suited to engraft and persist in a new host environment.⁴⁰ We show that, similarly, *Bt* casts

one metabolic phase that prioritized carbohydrate transport and metabolism,⁹ our time-course data suggest that *Bt* undergoes a temporally dynamic adaptational program. We show that *Bt* prioritizes biosynthesis of amino acids and other essential compounds early in colonization, before ramping up expression of a diverse array of PULs and ultimately centering metabolism around degradation of a single abundant dietary carbohydrate. This may reflect a transition from an initial stress response during establishment in the gut to a more growth-focused strategy that surveys and optimizes utilization of available environmental resources. We find that the set of genes required for *Bt* to initially establish colonization in the gut are distinct from those required to persist (Figure 1). The results presented here suggest that because of the rapidly shifting adaptational profile exhibited by microbial populations over the course of colonization, investigators must take care in selecting the appropriate time points to address their experimental questions.

a wide metabolic net upon gut entry, upregulating carbohydrate metabolism, energy metabolism, vitamin and cofactor biosynthesis, and especially amino acid biosynthesis. We likewise see that *Bt* upregulates a diverse array of PULs during early colonization (Figure 3). This may better enable *Bt* to survive conditions of resource scarcity until a more energetically efficient transcriptional program can be fine-tuned to the particulars of its new resource landscape.

Selection for efficient carbohydrate metabolism drives long-term persistence

During the later stages of colonization and persistence, *Bt* re-centers its metabolism around carbohydrate utilization. These results add to a growing body of work identifying metabolic necessity in general, and carbohydrate metabolism in particular, as powerful drivers of microbial fitness and evolution in the gut. For instance, one study showed that *E. coli* evolves mutations to

modulate carbohydrate utilization depending on dietary conditions,⁶ while another identified selection for mutations in either amino acid or carbohydrate metabolism depending on the competitive context.⁸ Research using *Bt* has demonstrated rapid evolution of divergent metabolic strategies depending on mouse diet.⁷ One study even showed how microbial competitive fitness in the mouse gut can be promoted by engineering a unique PUL into *Bt* and introducing the strain in combination with its associated carbohydrate substrate.⁴¹ Although microbes mediate competition in a number of ways ranging from direct attack to occupation of physical space to indirect interactions via the host,⁴² these findings collectively suggest that competition for scarce metabolic resources is a primary evolutionary battleground within and among microbial species in the gut ecosystem.

In these experiments, we identified strong selective pressure for improved utilization of a specific carbohydrate resource. However, previous work shows that genetic drift and transmission of microbes between hosts can significantly impact the evolution and spread of mutant populations.⁵ Therefore, it is important to consider how transmission between hosts may have impacted our results. In our RB-TnSeq experiments, mice were co-housed, facilitating intra-cage transmission. This may have artificially inflated the replicability of our results within cages, although we still saw near-identical trends emerge across four independent experiments and eight independent cages.

Changes in microbial localization and metabolic gene expression profile correlate

We found that changes in *Bt* resource use over the course of colonization paralleled shifts in its localization from the inner mucus layer toward the luminal space (Figure 6). This aligns with previous work showing that the mucus of GF mice is permeable to bacteria and takes up to 6 weeks of conventionalization to fully mature into the impermeable protective state that excludes *Bt* and most other gut commensals.^{43,44} Although we provide only correlational evidence here and causal experimentation is beyond the scope of this work, we hypothesize that the local microenvironment may dictate the selective pressures that ultimately drive *Bt* gene expression and evolution: *Bt* is known to use mucosal glycans only as a carbohydrate resource of last resort.⁴⁵ However, *Bt* that gets trapped in the permeable immature mucus layer early in colonization may not have direct access to luminal dietary resources. Under these resource-limited conditions, the population of mucus-embedded *Bt* may upregulate various PULs for consumption of mucosal glycans, as has been demonstrated in other *in vivo* mouse studies of *Bt* under conditions of dietary resource deficiencies.^{9,45–48} As the mucus layer matures and *Bt* gradually moves into the lumen, its metabolism shifts from broad mucosal glycan foraging while embedded (D2/D4) toward hyperutilization of a single abundant dietary resource while excluded (days 7–42).

Although more rigorous follow-up is needed to establish a causal relationship between localization and resource use, the correlation reported here provides preliminary support for the notion that the spatial localization and metabolic profile of *Bt* are deeply intertwined, flexible, and highly responsive to the specific balance of selective pressures such as resource availability

and energetic efficiency. These factors will doubtless be heavily impacted by the presence of additional community members. Nevertheless, we conclude that resource-use profiling and localization may emerge as particularly informative descriptors of available niche space in the gut.

IS3 transposable elements: A novel mechanism to modulate expression of specific CAZymes?

In GF mice fed a standard RFO-rich diet, the selective pressure for mutants with increased α -galactosidase activity is intense. Mutations in the BT1871 locus were consistently positively selected when WT *Bt* evolved in mice for 6 weeks. In all three mutant populations, the downstream side of the duplicated region ends midway through a ribosomal gene, meaning that there are no known transcriptional terminators between the ribosomal promoter and the α -galactosidase gene, BT1871. It is likely that these mutants increased α -galactosidase activity due to read-through from the strong ribosomal promoter in the upstream copy of the locus. Although increased α -galactosidase expression could be simply due to the presence of two copies of BT1871, the growth phenotype that these mutants exhibit, in which log-phase growth is five times faster than in WT, is on par with that of the RB-Tn mutants, for which α -galactosidase expression was more than ten times greater than in WT.

In *Bt*, identical copies of this IS3 transposable element occur in seven locations, often adjacent to PULs and almost always paired with a ribosomal gene. These genes were upregulated at D2/D4 of our transcriptomics experiment, shortly before we saw extensive upregulation of PUL24 genes. It is well known in both mammals and prokaryotes that transposable elements can modulate the expression of nearby and distant genes.⁴⁹ Transposable elements may be selected for because the genetic “cargo” that they shuttle along (such as an antibiotic cassette) is beneficial to the organism or because the position where the insertion occurs results in some downstream effect that is beneficial to fitness. Both reasons may contribute to the selection of the tandem duplication of the BT1871 locus. Future studies will be necessary to investigate whether other IS3 elements in *Bt* perform similar functions in modulating expression of nearby genes and whether such a mechanism can be found in other families of bacteria.

Limitations of the study

One limitation of this study is that many microbial genes are poorly annotated. At most of our transcriptomic time points, only a minority of the DEGs have known annotations, but those unannotated genes may still serve meaningful adaptive functions. These genes (Table S5B) would be excellent candidates for continued functional characterization through controlled *in vitro* and *in vivo* experiments. We also note the key limitation that this study was performed in a highly simplified monocolonization model. While these results provide evidence of general eco-evolutionary principles and highlight important considerations for understanding microbial GI colonization more broadly—e.g., the dynamism of the adaptational process and the importance of choosing time points carefully, the remarkable genetic mutability of bacteria, and the feedback cycles between a microbe and its resource environment—the specific results

presented here may not directly apply to scenarios with more complex microbial communities. However, by eventually comparing these results to those from more complex communities, this dataset can provide even greater insight into how host-microbe interactions and inter- and intraspecific microbial interactions each contribute to the adaptational process.

STAR★METHODS

Detailed methods are provided in the online version of this paper and include the following:

- **KEY RESOURCES TABLE**
- **RESOURCE AVAILABILITY**
 - Lead contact
 - Materials availability
 - Data and code availability
- **EXPERIMENTAL MODEL AND STUDY PARTICIPANT DETAILS**
 - Animals
 - Bacterial strains and growth conditions
- **METHOD DETAILS**
 - *In vivo* transcriptomic experiments
 - *In vivo* genome-wide mutant fitness assays
 - Isolation of mutants from fecal matter
 - Host-associated evolution of spontaneous *Bt* mutants
 - Isolate genome sequencing, assembly, and polishing
 - Metabolite extraction from cecal material
 - Metabolite analysis using GC-EI-MS and methoxyamine and TMS derivatization
 - RT-qPCR
 - ELISA
 - Histological procedures
 - Immunostaining and imaging
- **QUANTIFICATION AND STATISTICAL ANALYSIS**
 - PCoA, differential expression analysis, and Gene Set Enrichment Analysis (GSEA) on transcriptomic data
 - Pipeline for measuring relative abundance and fitness scores of RB-Tn mutants
 - Metabolomics statistics
 - Bacterial growth rate statistics
 - Genome mapping and coverage visualization
 - BT1871 copy number
 - Image quantification

SUPPLEMENTAL INFORMATION

Supplemental information can be found online at <https://doi.org/10.1016/j.celrep.2023.113009>.

ACKNOWLEDGMENTS

We thank Hualan Liu for invaluable experimental help with the RB-TnSeq libraries. We thank David Hershey and A. Murat Eren for helpful scientific input. We also thank the Chang lab members for scientific support received. The graphical abstract was created using BioRender. This work was performed with support from NIH T32DK007074 (M.Z., M.S.K.), NIH RC2DK122394 (E.B.C.), NIH T32GM007281 (M.S.K.), and the Host-Microbe and Tissue and Cell Engineering cores of the UChicago DDRCC, Center for Interdisciplinary Study of Inflammatory Intestinal Disorders (C-IID) (NIDDK P30 DK042086).

AUTHOR CONTRIBUTIONS

Conceptualization, M.S.K., M.Z., E.B.C., and J.B.; methodology, M.S.K., M.Z., and E.B.C.; formal analysis, M.S.K., M.Z., O.D., F.T., and A.M.S.; investigation, M.S.K., M.Z., J.B., K.L., S.T., K.T.C., A.M.S., and J.L.; resources, A.D.; data curation, M.S.K. and M.Z.; writing – original draft, M.S.K. and M.Z.; writing – review & editing, M.S.K., M.Z., E.B.C., A.F., J.B., C.H., and P.A.R.; visualization, M.S.K., M.Z., O.D., and F.T.; funding acquisition, E.B.C.

DECLARATION OF INTERESTS

The authors declare no competing interests.

INCLUSION AND DIVERSITY

We support inclusive, diverse, and equitable conduct of research.

Received: May 8, 2022

Revised: May 17, 2023

Accepted: August 3, 2023

Published: August 21, 2023

REFERENCES

1. O'Malley, M.A. (2007). The nineteenth century roots of “everything is everywhere.” *Nat. Rev. Microbiol.* 5, 647–651. <https://doi.org/10.1038/nrmicro1711>.
2. Goodman, A.L., McNulty, N.P., Zhao, Y., Leip, D., Mitra, R.D., Lozupone, C.A., Knight, R., and Gordon, J.I. (2009). Identifying Genetic Determinants Needed to Establish a Human Gut Symbiont in Its Habitat. *Cell Host Microbe* 6, 279–289. <https://doi.org/10.1016/j.chom.2009.08.003>.
3. Liu, H., Shiver, A.L., Price, M.N., Carlson, H.K., Trotter, V.V., Chen, Y., Escalante, V., Ray, J., Hern, K.E., Petzold, C.J., et al. (2021). Functional genetics of human gut commensal *Bacteroides thetaiotaomicron* reveals metabolic requirements for growth across environments. *Cell Rep.* 34, 108789. <https://doi.org/10.1016/j.celrep.2021.108789>.
4. Wu, M., McNulty, N.P., Rodionov, D.A., Khoroshkin, M.S., Griffin, N.W., Cheng, J., Latreille, P., Kerstetter, R.A., Terrapon, N., Henrissat, B., et al. (2015). Genetic determinants of *in vivo* fitness and diet responsiveness in multiple human gut *Bacteroides*. *Science* 350, aac5992. <https://doi.org/10.1126/SCIENCE.AAC5992>.
5. Vasequez, K.S., Willis, L., Cira, N.J., Ng, K.M., Pedro, M.F., Aranda-Díaz, A., Rajendram, M., Yu, F.B., Higginbottom, S.K., Neff, N., et al. (2021). Quantifying rapid bacterial evolution and transmission within the mouse intestine. *Cell Host Microbe* 29, 1454–1468.e4. <https://doi.org/10.1016/j.chom.2021.08.003>.
6. Crook, N., Ferreira, A., Gasparini, A.J., Pesesky, M.W., Gibson, M.K., Wang, B., Sun, X., Condiotte, Z., Dobrowolski, S., Peterson, D., and Dantas, G. (2019). Adaptive strategies of the candidate probiotic *E. coli* Nissle in the mammalian gut. *Cell Host Microbe* 25, 499–512.e8. <https://doi.org/10.1016/J.CHOM.2019.02.005>.
7. Dapa, T., Ramiro, R.S., Pedro, M.F., Gordo, I., and Xavier, K.B. (2022). Diet leaves a genetic signature in a keystone member of the gut microbiota. *Cell Host Microbe* 30, 183–199.e10. <https://doi.org/10.1016/J.CHOM.2022.01.002>.
8. Barroso-Batista, J., Pedro, M.F., Sales-Dias, J., Pinto, C.J.G., Thompson, J.A., Pereira, H., Demengeot, J., Gordo, I., and Xavier, K.B. (2020). Specific Eco-evolutionary Contexts in the Mouse Gut Reveal *Escherichia coli* Metabolic Versatility. *Curr. Biol.* 30, 1049–1062.e7. <https://doi.org/10.1016/j.cub.2020.01.050>.
9. Sonnenburg, J.L., Xu, J., Leip, D.D., Chen, C.H., Westover, B.P., Weatherford, J., Buhler, J.D., and Gordon, J.I. (2005). Glycan foraging *in vivo* by an intestine-adapted bacterial symbiont. *Science* (New York, N.Y.) 307, 1955–1959. <https://doi.org/10.1126/SCIENCE.1109051>.

10. Sonnenburg, J.L., Chen, C.T.L., and Gordon, J.I. (2006). Genomic and Metabolic Studies of the Impact of Probiotics on a Model Gut Symbiont and Host. *PLoS Biol.* 4, e413. <https://doi.org/10.1371/journal.pbio.0040413>.
11. Mahowald, M.A., Rey, F.E., Seedorf, H., Turnbaugh, P.J., Fulton, R.S., Wollam, A., Shah, N., Wang, C., Magrini, V., Wilson, R.K., et al. (2009). Characterizing a model human gut microbiota composed of members of its two dominant bacterial phyla. *Proc. Natl. Acad. Sci. USA* 106, 5859–5864. <https://doi.org/10.1073/pnas.0901529106>.
12. Becattini, S., Sorbara, M.T., Kim, S.G., Littmann, E.L., Dong, Q., Walsh, G., Wright, R., Amoretti, L., Fontana, E., Hohl, T.M., and Pamer, E.G. (2021). Rapid transcriptional and metabolic adaptation of intestinal microbes to host immune activation. *Cell Host Microbe* 29, 378–393.e5. <https://doi.org/10.1016/j.chom.2021.01.003>.
13. Donaldson, G.P., Chou, W.C., Manson, A.L., Rogov, P., Abeel, T., Bochicchio, J., Ciulla, D., Melnikov, A., Ernst, P.B., Chu, H., et al. (2020). Spatially distinct physiology of *Bacteroides fragilis* within the proximal colon of gnotobiotic mice. *Nat. Microbiol.* 5, 746–756. <https://doi.org/10.1038/s41564-020-0683-3>.
14. Wetmore, K.M., Price, M.N., Waters, R.J., Lamson, J.S., He, J., Hoover, C.A., Blow, M.J., Bristow, J., Butland, G., Arkin, A.P., and Deutschbauer, A. (2015). Rapid Quantification of Mutant Fitness in Diverse Bacteria by Sequencing Randomly Bar-Coded Transposons. *mBio* 6, e00306–e00315. <https://doi.org/10.1128/MBIO.00306-15>.
15. Irving, S.E., Choudhury, N.R., and Corrigan, R.M. (2021). The stringent response and physiological roles of (pp)pGpp in bacteria. *Nat. Rev. Microbiol.* 19, 256–271. <https://doi.org/10.1038/s41579-020-00470-y>.
16. Schofield, W.B., Zimmermann-Kogadeeva, M., Zimmermann, M., Barry, N.A., and Goodman, A.L. (2018). The Stringent Response Determines the Ability of a Commensal Bacterium to Survive Starvation and to Persist in the Gut. *Cell Host Microbe* 24, 120–132.e6. <https://doi.org/10.1016/j.chom.2018.06.002>.
17. Martens, E.C., Chiang, H.C., and Gordon, J.I. (2008). Mucosal glycan foraging enhances fitness and transmission of a saccharolytic human gut bacterial symbiont. *Cell Host Microbe* 4, 447–457. <https://doi.org/10.1016/j.chom.2008.09.007>.
18. Wexler, A.G., and Goodman, A.L. (2017). An insider's perspective: *Bacteroides* as a window into the microbiome. *Nat. Microbiol.* 2, 17026. <https://doi.org/10.1038/nmicrobiol.2017.26>.
19. El Kaoutari, A., Armougom, F., Gordon, J.I., Raoult, D., and Henrissat, B. (2013). The abundance and variety of carbohydrate-active enzymes in the human gut microbiota. *Nat. Rev. Microbiol.* 11, 497–504. <https://doi.org/10.1038/nrmicro3050>.
20. Drula, E., Garron, M.-L., Dogan, S., Lombard, V., Henrissat, B., and Terrapon, N. (2022). The carbohydrate-active enzyme database: functions and literature. *Nucleic Acids Res.* 50, D571–D577. <https://doi.org/10.1093/nar/gkab1045>.
21. Varel, V.H., and Bryant, M.P. (1974). Nutritional Features of *Bacteroides fragilis* subsp. *fragilis*. *Appl. Microbiol.* 28, 251–257.
22. Adamberg, K., Adamberg, S., Ernits, K., Larionova, A., Voor, T., Jaagura, M., Visnapuu, T., and Alamäe, T. (2018). Composition and metabolism of fecal microbiota from normal and overweight children are differentially affected by melibiose, raffinose and raffinose-derived fructans. *Anaerobe* 52, 100–110. <https://doi.org/10.1016/j.anaerobe.2018.06.009>.
23. Johansson, M.E.V., Sjövall, H., and Hansson, G.C. (2013). The gastrointestinal mucus system in health and disease. *Nat. Rev. Gastroenterol. Hepatol.* 10, 352–361. <https://doi.org/10.1038/nrgastro.2013.35>.
24. Chandler, M., Fayet, O., Rousseau, P., Ton Hoang, B., and Duval-Valentin, G. (2015). Copy-out-Paste-in Transposition of IS911: A Major Transposition Pathway. *Microbiol. Spectr.* 3. <https://doi.org/10.1128/MICROBIOL-SPEC.MDNA3-0031-2014>.
25. Macpherson, A.J., and Harris, N.L. (2004). Interactions between commensal intestinal bacteria and the immune system. *Nat. Rev. Immunol.* 4, 478–485. <https://doi.org/10.1038/nri1373>.
26. Bunker, J.J., Erickson, S.A., Flynn, T.M., Henry, C., Koval, J.C., Meisel, M., Jabri, B., Antonopoulos, D.A., Wilson, P.C., and Bendelac, A. (2017). Natural polyreactive IgA antibodies coat the intestinal microbiota. *Science* 358, eaan6619. <https://doi.org/10.1126/science.aan6619>.
27. Peterson, D.A., McNulty, N.P., Guruge, J.L., and Gordon, J.I. (2007). IgA Response to Symbiotic Bacteria as a Mediator of Gut Homeostasis. *Cell Host Microbe* 2, 328–339. <https://doi.org/10.1016/j.chom.2007.09.013>.
28. Hapfelmeier, S., Lawson, M.A.E., Slack, E., Kirundi, J.K., Stoel, M., Heikenwalder, M., Cahenzli, J., Velykoredko, Y., Balmer, M.L., Endt, K., et al. (2010). Reversible Microbial Colonization of Germ-Free Mice Reveals the Dynamics of IgA Immune Responses. *Science* 328, 1705–1709. <https://doi.org/10.1126/science.1188454>.
29. Joglekar, P., Ding, H., Canales-Herrerias, P., Pasricha, P.J., Sonnenburg, J.L., and Peterson, D.A. (2019). Intestinal IgA Regulates Expression of a Fructan Polysaccharide Utilization Locus in Colonizing Gut Commensal *Bacteroides thetaiotaomicron*. *mBio* 10, 023244–19–e2419. <https://doi.org/10.1128/mBio.02324-19>.
30. Nakajima, A., Vogelzang, A., Maruya, M., Miyajima, M., Murata, M., Son, A., Kuwahara, T., Tsuruyama, T., Yamada, S., Matsuura, M., et al. (2018). IgA regulates the composition and metabolic function of gut microbiota by promoting symbiosis between bacteria. *J. Exp. Med.* 215, 2019–2034. <https://doi.org/10.1084/jem.20180427>.
31. Huus, K.E., Bauer, K.C., Brown, E.M., Bozorgmehr, T., Woodward, S.E., Serapio-Palacios, A., Boutin, R.C.T., Petersen, C., and Finlay, B.B. (2020). Commensal Bacteria Modulate Immunoglobulin A Binding in Response to Host Nutrition. *Cell Host Microbe* 27, 909–921.e5. <https://doi.org/10.1016/j.chom.2020.03.012>.
32. Mazmanian, S.K., Round, J.L., and Kasper, D.L. (2008). A microbial symbiosis factor prevents intestinal inflammatory disease. *Nature* 453, 620–625. <https://doi.org/10.1038/nature07008>.
33. Coyne, M.J., Chatzidakis, L., Paoletti, L.C., and Comstock, L.E. (2008). Role of glycan synthesis in colonization of the mammalian gut by the bacterial symbiont *Bacteroides fragilis*. *Proc. Natl. Acad. Sci. USA* 105, 13099–13104. <https://doi.org/10.1073/pnas.0804220105>.
34. Porter, N.T., Canales, P., Peterson, D.A., and Martens, E.C. (2017). A Subset of Polysaccharide Capsules in the Human Symbiont *Bacteroides thetaiotaomicron* Promote Increased Competitive Fitness in the Mouse Gut. *Cell Host Microbe* 22, 494–506.e8. <https://doi.org/10.1016/j.chom.2017.08.020>.
35. Human Microbiome Project Consortium (2012). Structure, function and diversity of the healthy human microbiome. *Nature* 486, 207–214. <https://doi.org/10.1038/nature11234>.
36. Qin, J., Li, R., Raes, J., Arumugam, M., Burgdorf, K.S., Manichanh, C., Nielsen, T., Pons, N., Levenez, F., Yamada, T., et al. (2010). A human gut microbial gene catalog established by metagenomic sequencing. *Nature* 464, 59–65. <https://doi.org/10.1038/NATURE08821>.
37. Kuwahara, T., Yamashita, A., Hirakawa, H., Nakayama, H., Toh, H., Okada, N., Kuhara, S., Hattori, M., Hayashi, T., and Ohnishi, Y. (2004). Genomic analysis of *Bacteroides fragilis* reveals extensive DNA inversions regulating cell surface adaptation. *Proc. Natl. Acad. Sci. USA* 101, 14919–14924. <https://doi.org/10.1073/pnas.0404172101>.
38. Guo, Y., Kitamoto, S., and Kamada, N. (2020). Microbial adaptation to the healthy and inflamed gut environments. *Gut Microb.* 12, 1857505. <https://doi.org/10.1080/19490976.2020.1857505>.
39. Townsend, G.E., Han, W., Schwalm, N.D., Hong, X., Bencivenga-Barry, N.A., Goodman, A.L., and Groisman, E.A. (2020). A Master Regulator of *Bacteroides thetaiotaomicron* Gut Colonization Controls Carbohydrate Utilization and an Alternative Protein Synthesis Factor. *mBio* 11, e03221-19. <https://doi.org/10.1128/MBIO.03221-19>.

40. Watson, A.R., Füssel, J., Veseli, I., DeLongchamp, J.Z., Silva, M., Trigodet, F., Lolans, K., Shaiber, A., Fogarty, E., Runde, J.M., et al. (2023). Metabolic independence drives gut microbial colonization and resilience in health and disease. *Genome Biol.* 24, 78. <https://doi.org/10.1186/s13059-023-02924-x>.
41. Shepherd, E.S., Deloache, W.C., Pruss, K.M., Whitaker, W.R., and Sonnenburg, J.L. (2018). An exclusive metabolic niche enables strain engraftment in the gut microbiota. *Nature* 557, 434–438. <https://doi.org/10.1038/s41586-018-0092-4>.
42. Hibbing, M.E., Fuqua, C., Parsek, M.R., and Peterson, S.B. (2010). Bacterial competition: surviving and thriving in the microbial jungle. *Nat. Rev. Microbiol.* 8, 15–25. <https://doi.org/10.1038/nrmicro2259>.
43. Johansson, M.E.V., Jakobsson, H.E., Holmén-Larsson, J., Schütte, A., Ermund, A., Rodríguez-Piñero, A.M., Arike, L., Wising, C., Svensson, F., Bäckhed, F., and Hansson, G.C. (2015). Normalization of Host Intestinal Mucus Layers Requires Long-Term Microbial Colonization. *Cell Host Microbe* 18, 582–592. <https://doi.org/10.1016/j.chom.2015.10.007>.
44. Johansson, M.E.V., Philipson, M., Petersson, J., Velich, A., Holm, L., and Hansson, G.C. (2008). The inner of the two Muc2 mucin-dependent mucus layers in colon is devoid of bacteria. *Proc. Natl. Acad. Sci. USA* 105, 15064–15069. <https://doi.org/10.1073/pnas.0803124105>.
45. Desai, M.S., Seekatz, A.M., Koropatkin, N.M., Kamada, N., Hickey, C.A., Wolter, M., Pudlo, N.A., Kitamoto, S., Terrapon, N., Muller, A., et al. (2016). A Dietary Fiber-Deprived Gut Microbiota Degrades the Colonic Mucus Barrier and Enhances Pathogen Susceptibility. *Cell* 167, 1339–1353.e21. <https://doi.org/10.1016/j.cell.2016.10.043>.
46. Earle, K.A., Billings, G., Sigal, M., Lichtman, J.S., Hansson, G.C., Elias, J.E., Amieva, M.R., Huang, K.C., and Sonnenburg, J.L. (2015). Quantitative Imaging of Gut Microbiota Spatial Organization. *Cell Host Microbe* 18, 478–488. <https://doi.org/10.1016/j.chom.2015.09.002>.
47. Hayase, E., Hayase, T., Jamal, M.A., Miyama, T., Chang, C.-C., Ortega, M.R., Ahmed, S.S., Karmouch, J.L., Sanchez, C.A., Brown, A.N., et al. (2022). Mucus-degrading Bacteroides link carbenapenems to aggravated graft-versus-host disease. *Cell* 185, 3705–3719.e14. <https://doi.org/10.1016/j.cell.2022.09.007>.
48. Sonnenburg, E.D., and Sonnenburg, J.L. (2014). Starving our Microbial Self: The Deleterious Consequences of a Diet Deficient in Microbiota-Accessible Carbohydrates. *Cell Metabol.* 20, 779–786. <https://doi.org/10.1016/j.cmet.2014.07.003>.
49. Siguier, P., Filée, J., and Chandler, M. (2006). Insertion sequences in prokaryotic genomes. *Curr. Opin. Microbiol.* 9, 526–531. <https://doi.org/10.1016/j.mib.2006.08.005>.
50. Miyoshi, J., Bobe, A.M., Miyoshi, S., Huang, Y., Hubert, N., Delmont, T.O., Eren, A.M., Leone, V., and Chang, E.B. (2017). Peripartum Antibiotics Promote Gut Dysbiosis, Loss of Immune Tolerance, and Inflammatory Bowel Disease in Genetically Prone Offspring. *Cell Rep* 20, 491–504. <https://doi.org/10.1016/j.celrep.2017.06.060>.
51. Kolmogorov, M., Yuan, J., Lin, Y., and Pevzner, P.A. (2019). Assembly of long, error-prone reads using repeat graphs. *Nat. Biotechnol.* 37, 540–546. <https://doi.org/10.1038/s41587-019-0072-8>.
52. Walker, B.J., Abeel, T., Shea, T., Priest, M., Abouelliel, A., Sakthikumar, S., Cuomo, C.A., Zeng, Q., Wortman, J., Young, S.K., and Earl, A.M. (2014). Pilon: An Integrated Tool for Comprehensive Microbial Variant Detection and Genome Assembly Improvement. *PLoS One* 9, e112963. <https://doi.org/10.1371/JOURNAL.PONE.0112963>.
53. R Core Team R: A Language and Environment for Statistical Computing. R Foundation for Statistical Computing.
54. Oksanen, J., Simpson, G., Blanchet, F., Kindt, R., Legendre, P., Minchin, P., O'Hara, R., Solymos, P., Stevens, M., Szocs, E., et al. (2022). *Vegan: Community Ecology Package*.
55. Love, M.I., Huber, W., and Anders, S. (2014). Moderated estimation of fold change and dispersion for RNA-seq data with DESeq2. *Genome Biol.* 15, 550. <https://doi.org/10.1186/s13059-014-0550-8>.
56. Eren, A.M., Kiehl, E., Shaiber, A., Veseli, I., Miller, S.E., Schechter, M.S., Fink, I., Pan, J.N., Yousef, M., Fogarty, E.C., et al. (2021). Community-led, integrated, reproducible multi-omics with anvi'o. *Nat. Microbiol.* 6, 3–6. <https://doi.org/10.1038/s41564-020-00834-3>.
57. Korotkevich, G., Sukhov, V., Budin, N., Shpak, B., Artyomov, M.N., and Sergushichev, A. (2021). Fast Gene Set Enrichment Analysis. *BioRxiv*, 060012. <https://doi.org/10.1101/060012>.
58. Hyatt, D., Chen, G.L., LoCascio, P.F., Land, M.L., Larimer, F.W., and Hauser, L.J. (2010). Prodigal: Prokaryotic gene recognition and translation initiation site identification. *BMC Bioinf.* 11, 119–211. <https://doi.org/10.1186/1471-2105-11-119/TABLES/5>.
59. Langmead, B., and Salzberg, S.L. (2012). Fast gapped-read alignment with Bowtie 2. *Nat. Methods* 9, 357–359. <https://doi.org/10.1038/nmeth.1923>.
60. Li, H., Handsaker, B., Wysoker, A., Fennell, T., Ruan, J., Homer, N., Marth, G., Abecasis, G., and Durbin, R.; 1000 Genome Project Data Processing Subgroup (2009). The Sequence Alignment/Map format and SAMtools. *Bioinformatics* 25, 2078–2079. <https://doi.org/10.1093/BIOINFORMATICS/BTP352>.
61. Li, H. (2018). Minimap2: pairwise alignment for nucleotide sequences. *Bioinformatics* 34, 3094–3100. <https://doi.org/10.1093/BIOINFORMATICS/BTY191>.
62. Robinson, J.T., Thorvaldsdóttir, H., Winckler, W., Guttman, M., Lander, E.S., Getz, G., and Mesirov, J.P. (2011). Integrative Genomics Viewer. *Nat. Biotechnol.* 29, 24–26. <https://doi.org/10.1038/NBT.1754>.
63. Trigodet, F., Lolans, K., Fogarty, E., Shaiber, A., Morrison, H.G., Barreiro, L., Jabri, B., and Eren, A.M. (2022). High molecular weight DNA extraction strategies for long-read sequencing of complex metagenomes. *Mol. Ecol. Resour.* 22, 1786–1802. <https://doi.org/10.1111/1755-0998.13588>.
64. McMurdie, P.J., and Holmes, S. (2013). phyloseq: An R Package for Reproducible Interactive Analysis and Graphics of Microbiome Census Data. *PLoS One* 8, e61217. <https://doi.org/10.1371/JOURNAL.PONE.0061217>.
65. Mazmanian, S.K. (2008). Capsular Polysaccharides of Symbiotic Bacteria Modulate Immune Responses During Experimental Colitis (2008). *J. Pediatr. Gastroenterol. Nutr.* 46, E11–E12. <https://doi.org/10.1097/01.mpg.0000313824.70971.a7>.
66. Lee, M.D. (2019). GToTree: a user-friendly workflow for phylogenomics. *Bioinformatics* 35, 4162–4164. <https://doi.org/10.1093/BIOINFORMATICS/BTZ188>.
67. Eddy, S.R. (2011). Accelerated Profile HMM Searches. *PLoS Comput. Biol.* 7, e1002195. <https://doi.org/10.1371/JOURNAL.PCBI.1002195>.
68. Tatusov, R.L., Fedorova, N.D., Jackson, J.D., Jacobs, A.R., Kiryutin, B., Koonin, E.V., Krylov, D.M., Mazumder, R., Mekhedov, S.L., Nikolskaya, A.N., et al. (2003). The COG database: an updated version includes eukaryotes. *BMC Bioinf.* 4, 41. <https://doi.org/10.1186/1471-2105-4-41>.
69. Kanehisa, M., and Goto, S. (2000). KEGG: Kyoto Encyclopedia of Genes and Genomes. *Nucleic Acids Res.* 28, 27–30. <https://doi.org/10.1093/NAR/28.1.27>.
70. Aramaki, T., Blanc-Mathieu, R., Endo, H., Ohkubo, K., Kanehisa, M., Goto, S., and Ogata, H. (2020). KofamKOALA: KEGG Ortholog assignment based on profile HMM and adaptive score threshold. *Bioinformatics* 36, 2251–2252. <https://doi.org/10.1093/BIOINFORMATICS/BTZ859>.
71. Altschul, S.F., Gish, W., Miller, W., Myers, E.W., and Lipman, D.J. (1990). Basic local alignment search tool. *J. Mol. Biol.* 215, 403–410. [https://doi.org/10.1016/S0022-2836\(05\)80360-2](https://doi.org/10.1016/S0022-2836(05)80360-2).

STAR★METHODS

KEY RESOURCES TABLE

REAGENT or RESOURCE	SOURCE	IDENTIFIER
Antibodies		
Goat polyclonal anti-IgA	Southern Biotech	Cat#OB1040-01
Goat anti-mouse IgA:HRP	BioRad	Cat#STAR137P
Rabbit polyclonal anti-mouse Muc2	Santa Cruz Biotechnology	Cat#sc-15334
Alexa Fluor 488 goat anti-rabbit IgG	Invitrogen	Cat#A-11008
Bacterial and Virus Strains		
<i>Bacteroides thetaiotaomicron</i> VPI-5482 wildtype	Gift from Deutschbauer lab	AMD595
RB-Tn mutant isolated from monocolonized mice with barcoded transposon insertion in BT1876	Gift from Deutschbauer lab	AMD595-derived RB-Tn library ³
RB-Tn mutant isolated from monocolonized mice with barcoded transposon insertion in BT1874	This work	Tn_BT1874
RB-Tn mutant isolated from monocolonized mice with barcoded transposon insertion in BT1876	This work	Tn_BT1876
RB-Tn mutant isolated from monocolonized mice with barcoded transposon insertion in the intergenic region between BT1872 and BT1873	This work	Tn_BT1872-83
RB-Tn mutant isolated from monocolonized mice with barcoded transposon insertion in BT1872	This work	Tn_BT1872
RB-Tn mutant isolated from monocolonized mice with barcoded transposon insertion in BT1874 and BT3132	This work	Tn_BT1874/BT3132
RB-Tn mutant isolated from monocolonized mice with barcoded transposon insertion in BT3133	This work	Tn_BT3133
WT <i>Bt</i> with a copy of BT1871 integrated into the <i>Bt</i> genome at the attN1 site under the BT1311 (<i>rpoD</i>) constitutive promoter.	This work	WT + BT1871OE
<i>Bt</i> mutant isolated from feces after 6-week monoassociation of <i>Bt</i> ; carries a tandem repeat of the BT1871 locus (see Figure 7).	This work	MZ65
Chemicals, Peptides, and Recombinant Proteins		
Brain Heart Infusion Broth	Fisher	Cat#DF0037178
Agar	Fisher	Cat#DF0145-17-0
Hemin	Fisher	Cat#51280-5G
Glucose	Sigma	Cat#158968-500G
Galactose	Sigma	Cat#G0750-500G
Sucrose	Fisher	Cat#AAJ64270A1
Raffinose	Fisher	Cat#AC195670250
Melibiose	Sigma	Cat#M5500-100G
Erythromycin	Fisher	Cat#AC227330050
Phosphate Buffered Saline	Sigma	Cat#P3813-10PAK
Glycerol	Fisher	Cat#BP2291

(Continued on next page)

Continued

REAGENT or RESOURCE	SOURCE	IDENTIFIER
Ambion TRIzol Reagent	Fisher	Cat#15-596-018
Chloroform	Fisher	Cat#AC390760010
Isopropanol	Fisher	Cat#BP2618500
Ethanol	Fisher	Cat#BP2818500
DNAse	Fisher	Cat#18068015
Tris	Fisher	Cat#BP152-10
EDTA	Fisher	Cat#PR-V4231
NaCl	Fisher	Cat#S640-10
SDS	Sigma	Cat#L3771-25G
Phenol:Chloroform:Isoamyl Alcohol	Fisher	Cat#AM9732
Proteinase K	Sigma	Cat#3115852001
HCl	Sigma	Cat#A144-212
Methanol	Fisher	Cat#A452SK-4
Methoxyamine	Sigma	Cat#226904
Pyridine	Sigma	Cat#270970
Derivatizing reagent (BSTFA +1% TMCS)	Sigma	Cat#B-023
Ethyl acetate	Sigma	Cat#650528
ELISA diluent	R&D Systems	Cat#DY995
Acetic acid	Fisher	Cat#A38-500
Xylene	Fisher	Cat#X3S-4
Lysozyme	Fisher	Cat#89833
Sodium citrate	Fisher	Cat#S279-500
DAPI	Sigma	Cat#D8417-5MG
ProLong Gold Anti-Fade mounting medium	Fisher	Cat#P10144
iTaq Universal SYBR Green Supermix	BioRad	Cat#1725124

Critical Commercial Assays

DNeasy PowerSoil Kit.	Qiagen	Cat#47016
Rapid Barcoding Kit	Oxford Nanopore Technologies	Cat#SQK-RBK004
Transcriptor First Strand cDNA Synthesis Kit	Roche	Cat#35081963001
Invitrogen IgG (Total) Mouse Uncoated ELISA Kit	Invitrogen	Cat#88-50400-88

Deposited Data

RNAseq raw data from <i>Bt</i> at different time points	This work	https://www.ncbi.nlm.nih.gov/sra (accession: PRJNA797447)
Shotgun sequencing raw data from evolution experiment fecal samples	This work	https://www.ncbi.nlm.nih.gov/sra (accession: PRJNA797447)
Long-read sequencing raw data from isolate MZ65	This work	https://www.ncbi.nlm.nih.gov/sra (accession: PRJNA797447)

Experimental Models: Organisms/Strains

Mouse: germ-free wild-type C57BL/6J	University of Chicago Gnotobiotic Core Facility	N/A
-------------------------------------	---	-----

Oligonucleotides

Custom Ribo-Zero Plus Probes	SeqCenter	See Table S1A
qPCR primers	Miyoshi et al., 2017 ⁵⁰	See Table S1B

Software and Algorithms

bcl2fastq	Illumina	Version 2.20.0.422
MinKNOW	Oxford Nanopore Technologies	Version 4.3.4
Guppy	Oxford Nanopore Technologies	Version 5.0.11

(Continued on next page)

Continued

REAGENT or RESOURCE	SOURCE	IDENTIFIER
Flye	https://github.com/fenderglass/Flye	Version 2.6 ⁵¹
Pilon	https://github.com/broadinstitute/pilon	Version 1.23 ⁵²
MassHunter Quantitative Analysis software	Agilent Technologies	Version B.10
R software	https://www.r-project.org/	Version 4.2.1 ⁵³
vegan R software	https://cran.r-project.org/web/packages/vegan/index.html	Version 2.6–4 ⁵⁴
pairwiseAdonis R software	https://github.com/pmartinezarbizu/pairwiseAdonis	Version 0.4
DESeq2 R software	https://bioconductor.org/packages/release/bioc/html/DESeq2.html	Version 1.36.0 ⁵⁵
anvi'o	https://anvio.org/	Version 7.1 ⁵⁶
fgsea R package	https://bioconductor.org/packages/release/bioc/html/fgsea.html	Version 3.17 ⁵⁷
Graphpad Prism	https://www.graphpad.com/features	Version 9
Prodigal	https://github.com/hyatt/Prodigal	Version 2.6.3 ⁵⁸
bowtie2	https://bowtie-bio.sourceforge.net/bowtie2/index.shtml	Version v2.3.5.1 ⁵⁹
samtools	http://www.htslib.org/	Version 1.11 ⁶⁰
gggenes	https://github.com/wilkox/gggenes/tree/master	Version 0.4.1
blastn	https://blast.ncbi.nlm.nih.gov/Blast.cgi	Version 2.5.0
minimap2	https://github.com/lh3/minimap2	Version 2.17 ⁶¹
IgV	https://igv.org/	Version 2.11.1 ⁶²
LAS_X Leica	Leica	N/A
Other		
Standard mouse chow	LabDiets	5K67
Anaerobic chamber	Coy Laboratory Products	N/A
GENSYS 40-Vis spectrophotometer	Thermo Scientific	N/A
Mini-BeadBeater-96	BioSpec Products	N/A
BioAnalyzer	Agilent	N/A
NextSeq2000	Illumina	N/A
IsoCage P Bioexclusion cages	Tecniplast	N/A
Agencourt AMPure XP beads	Beckman Coulter	Cat#A63882
Flow Cell (R9.4.1)	Oxford Nanopore Technologies	Cat#FLO-MIN106D
MinION	Oxford Nanopore Technologies	N/A
Beadruptor tubes	Fisher	Cat#15-340-154
Bead Mill 24 Homogenizer	Fisher	Cat#15-340-163
Mass spectrometry autosampler vial	Microliter	Cat#09-1200
Biotage SPE Dry 96 Dual	Biotage	Cat#3579M
Thermomixer C	Eppendorf	Cat#2231001005
Agilent 7890A GC system	Agilent	N/A
Agilent 5975C MS detector	Agilent	N/A
HP-5MSUI column	Agilent	Cat#19091S-433UI
CFX384 Real-Time System	BioRad	N/A
Leica SP8 laser scanning confocal microscope	Leica	N/A

RESOURCE AVAILABILITY

Lead contact

Further information and requests for resources and reagents may be directed to and will be fulfilled by the lead contact, Eugene Chang (echang@medicine.bsd.uchicago.edu).

Materials availability

Bacterial strains obtained in this study will be made available upon request addressed to the [lead contact](#).

Data and code availability

- All sequencing data, including DNA and RNA datasets, have been deposited at NCBI Sequence Read Archive and are publicly available as of the date of publication. Accession numbers are listed in the [key resources table](#).
- This paper does not report original code.
- Any additional information required to reanalyze the data reported in this paper is available from the [lead contact](#) upon request.

EXPERIMENTAL MODEL AND STUDY PARTICIPANT DETAILS

Animals

Female 8–12 week-old C57Bl/6J germ-free mice were bred and maintained in plastic gnotobiotic isolators or bioexclusion racks within the University of Chicago Gnotobiotic Core Facility and fed *ad libitum* autoclaved standard chow diet (LabDiets 5K67). Litter-mates were randomly assigned to treatment groups. All murine experimental procedures were institutionally approved.

Bacterial strains and growth conditions

The bacterial strains used in this study, including the RB-TnSeq library, are listed in the Key Resources Table. *Bacteroides thetaio-tamicron* VPI-5482 [AMD595], and all its derivatives were cultured anaerobically at 37°C in liquid Brain Heart Infusion Supplemented (BHI-S) medium or defined Varel-Bryant medium as described in Liu et al.,³ and Varel and Bryant.²¹ Varel-Bryant medium with no carbon source was supplemented with glucose, galactose, sucrose, raffinose, or melibiose to a final concentration of 20 mM. An anaerobic chamber (Coy Laboratory Products) filled from tanks containing 10% CO₂, 7.5% H₂, and 82.5% N₂ was used for all anaerobic microbiology procedures, with working conditions near 2–3% H₂.

For growth rate measurements, colonies of *Bt* were inoculated into 3 mL of BHI-S in plastic culture tubes and grown overnight at 37°C, for a total of 6 biological replicates. Immediately before inoculating with the cells, sealed Hungate tubes containing 10 mL of VB medium and a 20 mL headspace were inoculated via syringe with autoclaved sugar solution and hemin solution for a final concentration of 20 mM sugar and 5 µg/mL hemin. Overnight cultures were diluted to OD₆₀₀ = 1, and 100 µL of the diluted culture was inoculated into the prepared media tubes via syringe. Anaerobically sealed cultures were grown outside of the chamber in a 37°C incubator with no shaking. Every 45 min, the cultures were taken from the incubator, cells resuspended by shaking, and their OD₆₀₀ readings measured by a GENSYS 40-Vis spectrophotometer.

METHOD DETAILS

In vivo transcriptomic experiments

Mice were inoculated with a single dose of wildtype *Bt* VPI-5482 at 10⁶ – 10⁸ CFU/200 µL, and were then sacrificed at 0.5, 1, 2, 4, 7, 14, and 42 days post-colonization. Luminal contents of the mice cecum were immediately snap-frozen in liquid N₂ and stored at –80°C. About 50 mg of the contents were transferred into 2 mL screw-cap tubes, followed by the addition of 1 mL TRIzol reagent for the isolation of RNA. The samples were homogenized by beadbeating with 0.1 mm glass beads in a Mini-BeadBeater-96 for 2 min. Total RNA isolation and purification were performed using the TRI reagent protocol and quality checked by BioAnalyzer. All library preparation and sequencing work was performed by SeqCenter (Pittsburgh, PA). Initial DNase treatment is performed with Invitrogen DNase (RNAse free). Library preparation is performed using Illumina's Stranded Total RNA Prep Ligation with Ribo-Zero plus. Custom Ribo-Zero probes were designed for *Bt* and supplemented alongside the standard probe set. Custom probe sequences can be found in [Table S1](#). Sequencing was performed on a NextSeq2000 giving 2x50bp reads. Post sequencing, bcl2fastq (v2.20.0.422) was used to demultiplex and trim adaptors.

In vivo genome-wide mutant fitness assays

Four individual cohorts of mice were used, indicated by the month of the experiment. For each cohort, mice were housed in cages of 2–3 animals either within a gnotobiotic isolator (Dec, Jan) or in hermetically sealed Tecniplast IsoCage P Bioexclusion cages on a rack system (Mar, Oct), and allowed to acclimate for 3 days prior to colonization ([Figure S1A](#)). Mice were inoculated with a single dose of the *Bt* RB-TnSeq mutant library at 10⁶ – 10⁸ CFU/200 µL. The inoculum was prepared by one of two methods: 1) frozen 2 mL aliquots of the *Bt* RB-TnSeq library were thawed and gavaged directly into mice (Dec, Jan), or 2) a thawed 2 mL aliquot of the *Bt* RB-TnSeq library was grown in 150 mL BHI-S medium overnight with 20 µg/mL erythromycin (16 h), and backdiluted to OD₆₀₀ = 0.05 the next

morning to allow for fresh cells to reach mid-log phase (3 h) by the time of inoculation (Mar, Oct). For each experiment, at least 3 cell pellets of the inoculum were collected as Time = 0 references. Each mouse was colonized by oral gavage with 200 μ L of the *Bt* transposon library. Stool samples were collected daily (excluding weekends), up to 14 days post-colonization to assess longitudinal shifts in mutant abundance. Mice were monitored and weighed daily. Genomic DNA was extracted using the DNeasy PowerSoil Kit.

The IsoCage P rack system facilitated sample collection while maintaining gnotobiotic conditions, and although the fresh and frozen inocula exhibited nearly identical coverage of the *Bt* genome (Figure S1B) and harbored statistically indistinguishable levels of diversity (Figures S1C and S1D), use of fresh rather than frozen inoculum substantially reduced bottleneck effects, allowing for low-abundance mutants to reach the gut and persist at a much higher rate through at least D1 (Figure S1E), with diversity only beginning to decrease at D4 (Figure 4A). Because of the bottleneck effect in the frozen inoculum cohorts, analysis of early time points in the functional genetics experiments is restricted to experiments that used fresh inoculum (Mar, Oct). Results from later time points converged across all four runs of the experiment, in spite of differences in protocol (Figures 1C and 4E).

Isolation of mutants from fecal matter

Mouse feces were collected and immediately homogenized in 500 mL 25% glycerol solution and stored at -80°C . Prior to isolation, glycerol stocks were allowed to thaw on the benchtop for 10 min, centrifuged for 30 s at 2,000 RPM. On each 150 mm BHI-S plate, 100 μ L of 10^{-3} , 10^{-4} , or 10^{-5} dilution of the glycerol stock was spread using 4.5 mm glass beads. The plates were incubated anaerobically at 37°C for two days. Individual colonies were picked into 1 mL 96-well plates containing 750 μ L BHI-S in each well. After 16 h of growth, glycerol was added to a final concentration of 20% and the isolates were stored. The isolate stocks were used as the template in PCR amplifying the barcoded region of the mutants. The PCR products were sent for Sanger sequencing.

Host-associated evolution of spontaneous *Bt* mutants

Three female mice 8-12 wk-old C57Bl/6J GF mice were co-housed in the same gnotobiotic isolator and fed standard chow diet *ad libitum*, and were then given a single dose of wildtype *Bt* VPI-5482 at $10^6 - 10^8$ CFU/200 μ L. One week post inoculation of *Bt*, the three mice were separated into individual cages. A fecal sample was taken six weeks post inoculation. DNA was extracted from the fecal pellets by the phenol-chloroform method, followed by ethanol precipitation, and sent for shotgun sequencing. Individual isolates from each fecal pellet were cultured from the bulk material as outlined in Isolation of mutants from fecal matter. We assayed for isolates with increased growth in VB-melibiose and selected one isolate from each mouse for MinION long-read sequencing.

Isolate genome sequencing, assembly, and polishing

To provide greater context for the delineation of the complex chromosomal rearrangements associated with the BT1872/BT1873 operon, a long-read sequencing strategy was employed. The isolate genomes assessed were wildtype *Bt*, the strain used for the mouse experiments, and three spontaneous mutant cultivars (MZ55, MZ58 and MZ65), which demonstrated enhanced growth rates in the presence of melibiose, recovered from the feces of mice six weeks after initial inoculation. Total genomic HMW DNA was extracted by a standard phenol chloroform protocol on overnight 25 mL BHIS broth cultures.⁶³ DNA was resuspended in 0.1 mL 10 mM Tris-HCl, pH 8.5.

Slow pipetting, wide bore pipette tips and steps to minimize velocity gradients were implemented throughout to avoid further shearing of DNA molecules. Libraries were prepared with the Rapid Barcoding Kit (SQK-RBK004) and the standard protocols from Oxford Nanopore Technologies were used with the following modifications. DNA fragmentation was performed on 10 μ g DNA using 10 passes through a 22G needle in a 250 μ L volume before purification using 0.5% Agencourt AMPure XP beads (A63882, Beckman Coulter). Each elution step of the AMPureXP beads was performed using 10 mM Tris-Cl pH 8.5 instead of water, at 37°C for 5 min. The gDNA inputs into library preparation ranged between 0.5 μ g and 1.2 μ g (Table S2), based on sample availability in a standard 8.5 μ L volume, with 1.5 μ L Fragmentation mix added to each sample. Barcoded libraries were pooled so each sample contributed an equal input mass (~ 0.5 μ g). Using MinkNOW v4.3.4, a single R9.4/FLO-MIN106 flow cell (Oxford Nanopore Technologies) sequenced the final prepared library with a starting voltage of -180 mV and a run time of 72 h. Guppy v5.0.11 and the sup model were used for post-run basecalling, sample de-multiplexing and the conversion of raw FAST5 files to FASTQ files. For downstream analyses, we only used reads with a minimum quality score of 7. We assembled long-reads contigs with Flye.⁵¹ Additional DNA extractions were carried out for every isolate using a standard phenol-chloroform extraction and send for short-read sequencing. We then used the short-reads to polish the long-read assemblies using Pilon v1.23.⁵²

Metabolite extraction from cecal material

Metabolites were extracted with the addition of extraction solvent (80% methanol spiked with internal standards and stored at -80°C , Table S4) to pre-weighed fecal/cecal samples at a ratio of 100 mg of material per mL of extraction solvent in beadbeater tubes (Fisherbrand; 15-340-154). Samples were homogenized at 4°C on a Bead Mill 24 Homogenizer (Fisher; 15-340-163), set at 1.6 m/s with 6 30-s cycles, 5 s off per cycle. Samples were then centrifuged at -10°C , 20,000 \times g for 15 min and the supernatant was used for subsequent metabolomic analysis.

Metabolite analysis using GC-EI-MS and methoxyamine and TMS derivatization

Metabolites were analyzed using gas chromatography-mass spectrometry (GCMS) with electron impact ionization. To a mass spectrometry autosampler vial (Microliter; 09-1200), 100 μ L of metabolite extract was added and dried down completely under a nitrogen

stream at 30 L/min (top) and 1 L/min (bottom) at 30°C (Biotage SPE Dry 96 Dual; 3579M). To dried samples, 50 μ L of freshly prepared 20 mg/mL methoxyamine (Sigma; 226904) in pyridine (Sigma; 270970) was added and incubated in a thermomixer C (Eppendorf) for 90 min at 30°C and 1400 rpm. After samples are cooled to room temperature, 80 μ L of derivatizing reagent (BSTFA +1% TMCS; Sigma; B-023) and 70 μ L of ethyl acetate (Sigma; 439169) were added and samples were incubated in a thermomixer at 70°C for 1 h and 1400 rpm. Samples were cooled to RT and 400 μ L of Ethyl Acetate was added to dilute samples. Turbid samples were transferred to microcentrifuge tubes and centrifuged at 4°C, 20,000 \times g for 15 min. Supernatants were then added to mass spec vials for GCMS analysis. Samples were analyzed using a GC-MS (Agilent 7890A GC system, Agilent 5975C MS detector) operating in electron impact ionization mode, using an HP-5MSUI column (30 m \times 0.25 mm, 0.25 μ m; Agilent Technologies 19091S-433UI) and 1 μ L injection. Oven ramp parameters: 1 min hold at 60°C, 16°C per min up to 300°C with a 7 min hold at 300°C. Inlet temperature was 280°C and transfer line was 300°C. Data analysis was performed using MassHunter Quantitative Analysis software (version B.10, Agilent Technologies) and confirmed by comparison to authentic standards. Normalized peak areas were calculated by dividing raw peak areas of targeted analytes by averaged raw peak areas of internal standards.

RT-qPCR

Total messenger RNA was isolated from colonic mucosal scrapings with TRIzol reagent according to the same protocol used for cecal RNA isolation. Transcriptor First Strand cDNA Synthesis Kit (Roche Diagnostics Corporation) was used to obtain cDNA. Real-time qPCR was performed using iTaq Universal SYBR Green Supermix with CFX384 Real-Time System (Bio-Rad). Primers are listed in [Table S1](#).

ELISA

For cecal IgA ELISA, frozen cecal samples were resuspended in 1 mL of ELISA diluent per 100mg of cecal contents and homogenized by bead beating for 1 min. ELISA was performed using goat polyclonal anti-IgA antibody (capture antibody) (Southern Biotech: 1040-01) and goat anti-IgA antibody labeled with HRP (secondary antibody) (Bio-Rad: STAR137P). IgG ELISA was performed on frozen serum samples using Invitrogen IgG (Total) Mouse Uncoated ELISA Kit.

Histological procedures

During sacrifice of mice colonized with WT *Bt* for transcriptomics experiments, distal colonic cross-sections were collected and placed in cassettes. Tissues were fixed by immersion in Carnoy's solution (60% ethanol, 30% chloroform, 10% acetic acid) for 3 h and were stored in 70% ethanol until tissue sectioning. When ready to process, samples were dehydrated by two successive washes each in methanol for 35 min, ethanol for 30 min, and xylene for 25 min. Tissue samples within cassettes were then submerged in melted paraffin at 68°C for 1hr, removed, and kept at room temperature until sectioning. Paraffin blocks were cut into 4- μ m-thick sections and deparaffinized for immunofluorescence.

Immunostaining and imaging

After deparaffinization and rehydration, slides were incubated in lysozyme solution at 37°C for 20 min, and then in antigen retrieval solution (10 mM sodium citrate [pH 6.0]) at 90°C for 10 min. For mucus visualization, a polyclonal rabbit anti-mouse Muc2-specific antibody (Santa Cruz Biotechnology) was diluted 1:100 in blocking buffer (Dako), applied to the slide, and incubated for 2 h in the dark at room temperature. Slides were washed gently three times in TBS-T. The secondary antibody (Alexa Fluor 488 goat anti-rabbit IgG, Invitrogen) was diluted 1:100 in blocking buffer, applied to the slide, and incubated for 30 min in the dark at room temperature. Slides were again washed gently three times in TBS-T, and were then stained with DAPI 10 μ g/mL (Sigma), incubated for 1 min, and washed three times in PBS. Slides were then dried, mounted with ProLong Gold Anti-Fade mounting medium (Invitrogen) and stored at room temperature in the dark until imaging. Images were acquired on a Leica SP8 laser scanning confocal microscope with the LAS_X Leica software (Leica). All samples were imaged with a 40 \times oil-immersion objective. Images were acquired at a frame size of 1024 \times 1024 with 16-bit depth.

QUANTIFICATION AND STATISTICAL ANALYSIS

PCoA, differential expression analysis, and Gene Set Enrichment Analysis (GSEA) on transcriptomic data

The R⁵³ package 'phyloseq'⁶⁴ was used to calculate Bray-Curtis dissimilarity for all pairwise combinations of transcriptome samples, which was then ordinated to create PCoA plots. PERMANOVA analysis using the R package 'vegan' was performed to evaluate sample clustering by experimental day with significance criteria set at $p < 0.05$. Post-hoc pairwise PERMANOVA analyses using FDR method to correct for multiple testing ('pairwiseAdonis') were then performed to evaluate significant pairwise differences in clustering ([Table S3](#)).

Gene calls were mapped to KEGG ortholog (Kofam) annotations in R. Differential expression analysis of each gene call was performed by pairwise comparisons with 'deseq2',⁵⁵ with the significance criteria $\log(\text{FDR-adjusted } p \text{ value}) < -3$, $|\log_2(\text{fold change})| > 2$, and max group mean > 50 RPM. Metabolism for the *Bt* genome was estimated using the anvi'o v7.1 program 'anvi-estimate-genome.' Gene calls for each metabolic pathway found within the *Bt* genome were then transferred into a unique GSEA pathway query list in R ('fgsea'),⁵⁷ and pathway enrichment was then calculated using the differential expression statistics calculated with 'deseq2'.⁵⁵ Pathways were filtered for $\text{padj} < 0.05$ and the normalized enrichment scores (NES) was plotted (PRISMv9). Other custom gene lists were created to calculate the enrichment of other gene sets including the polysaccharide utilization loci (PULs),²⁰ capsular polysaccharide

loci (CPSs),⁶⁵ and genes associated with the *Bt* stringent response.¹⁶ Statistical results from these RNAseq analyses are presented in Table S5.

Pipeline for measuring relative abundance and fitness scores of RB-Tn mutants

RB-TnSeq strain and gene fitness scores were calculated as described previously from strain-level count data (significance threshold: t -statistic $< -3\sigma$).¹⁴ For temporal abundance analyses of TnSeq mutants for each cohort, we first created a feature table with raw counts of strain-level mutants across each sample. This table was filtered to remove strains with counts of 1, as these are likely produced by sequencing error. Next, counts were normalized by the count of a synthetic spike-in barcode that was introduced at 20 p.m. into each sample during PCR amplification of the barcodes. Samples where the spike-in represented $>30\%$ of total reads were discarded. The synthetic spike-in barcode was subsequently removed as a feature from the table, and the resulting tables were used for alpha diversity analyses via the R package 'vegan'.⁵⁴ For all other relative abundance analyses, strains were assigned to genes based on previous mapping by Liu et al.,³ as well as manual mapping performed for this experiment. Strains that had not been mapped here or elsewhere were binned together as "non-mapping" strains, and strain-level counts were then summed for each gene. For all subsequent analyses, we further filtered out genes that mapped to *Bt* plasmids in order to focus on chromosomal gene fitness patterns. The R package 'phyloseq' was used to calculate Bray-Curtis dissimilarity for all pairwise combinations of samples, which was then used to create PCoA plots.⁶⁴ PERMANOVA analysis using the R package 'vegan' was performed to evaluate sample clustering by experimental day with significance criteria set at $p < 0.05$ (Table S3). Finally, filtered count tables were adjusted to relative abundance based on the total remaining counts, and used to track gene-level relative abundance over time. For linear regression of initial vs. final relative abundance of gene mutants, genes with zero-counts were re-assigned a relative abundance of 1×10^{-7} to perform log-transformation of the data.

Metabolomics statistics

As amino acid abundances (Figure 2E) were normalized within compounds and cannot be compared across compounds, for each metabolite, we performed one-way ANOVA across all time points, with post-hoc follow-up tests and FDR correction (Table S4). Carbohydrate metabolite abundances (Figures 5D, S3C and S3D) were compared within compounds across time points using one-way ANOVA with post-hoc follow-up tests and FDR correction (Table S6).

Bacterial growth rate statistics

Growth rates of different Tn mutant isolates (Figures 5A and S3B) were compared by one-way ANOVA with post-hoc follow-up tests and FDR correction (Table S6).

Genome mapping and coverage visualization

We used anvi'o v7.1⁵⁶ and the pangenomic workflow to compute and visualize genomic coverage for each isolate genome from the evolution experiments. Briefly, the workflow uses (1) Prodigal v2.6.3⁵⁸ to identify open-reading frames (ORFs), (2) 'anvi-run-hmm' to identify single copy core genes from bacteria ($n = 71$)⁶⁶ and ribosomal RNAs ($n = 12$, modified from¹) using HMMER v3.3.⁶⁷ (3) 'anvi-run-ncbi-cogs' and 'anvi-run-kegg-kofams' to annotate ORFs with the NCBI's Clusters of Orthologous Groups (COGs),⁶⁸ and the KOfam HMM database of KEGG orthologs (KOs)^{69,70} respectively. We used bowtie2 v2.3.5.1⁵⁹ to recruit short-reads to the contigs, and samtools v1.11⁶⁰ to convert SAM files to BAM files. We profiled the resulting BAM files with 'anvi-profile' and used the program 'anvi-merge' to combine all single profiles into a merged profile for downstream visualization. We used 'anvi-get-split-coverages' and 'anvi-script-visualize-split-coverages' to generate coverage plots. We used 'anvi-export-gene-calls' and gggenes v0.4.1 to visualize the genomic context around BT1871.

BT1871 copy number

We used blast⁷¹ to compute the number of long-reads with two copies of the BT1871 locus in the MZ65 isolate. We extracted the gene sequence (1989 bp) from the initial *Bt* genome (AMD595) using anvi'o interactive interface and used blastn v2.5.0 to blast the long-reads from MZ65. Blast hits with an alignment length $>180\%$ of the gene length were flagged as "two copies" and hits with alignment length between 80% and 105% were flagged as "one copy". To visualize long-reads with two copies of BT1871, we used minimap2 v2.17⁶¹ to map the MZ65 long-reads to the MZ65 genome, which had two copies of the BT1871 region. We used samtools v1.11 to extract the reads with two copies as identified above and used IGV v2.11.1⁶² to visualize the mapping and generate a figure.

Image quantification

For each mouse, a single colonic cross-section was used to generate 6 representative images. Images were masked to split the DAPI signal into an epithelial channel (blue) and a luminal channel (red). The MUC2 channel was green. To assess proximity of *Bt* to the epithelium, at 10 evenly-spaced points along the epithelium in each frame, a perpendicular line was drawn until it intersected the nearest bacterial cell, and this distance was measured. These measurements were averaged across all frames for each mouse. Average measurements of $n = 3-4$ mice per time point were used to compare *Bt* epithelial proximity across experimental days by performing one-way ANOVA and then post-hoc follow-up tests with FDR correction to compare all time points to D1. Differences were considered significant at $q < 0.05$.

Supplemental information

Dynamic genetic adaptation

of *Bacteroides thetaiotaomicron*

during murine gut colonization

Megan S. Kennedy, Manjing Zhang, Orlando DeLeon, Jacie Bissell, Florian Trigodet, Karen Lolans, Sara Temelkova, Katherine T. Carroll, Aretha Fiebig, Adam Deutschbauer, Ashley M. Sidebottom, Joash Lake, Chris Henry, Phoebe A. Rice, Joy Bergelson, and Eugene B. Chang

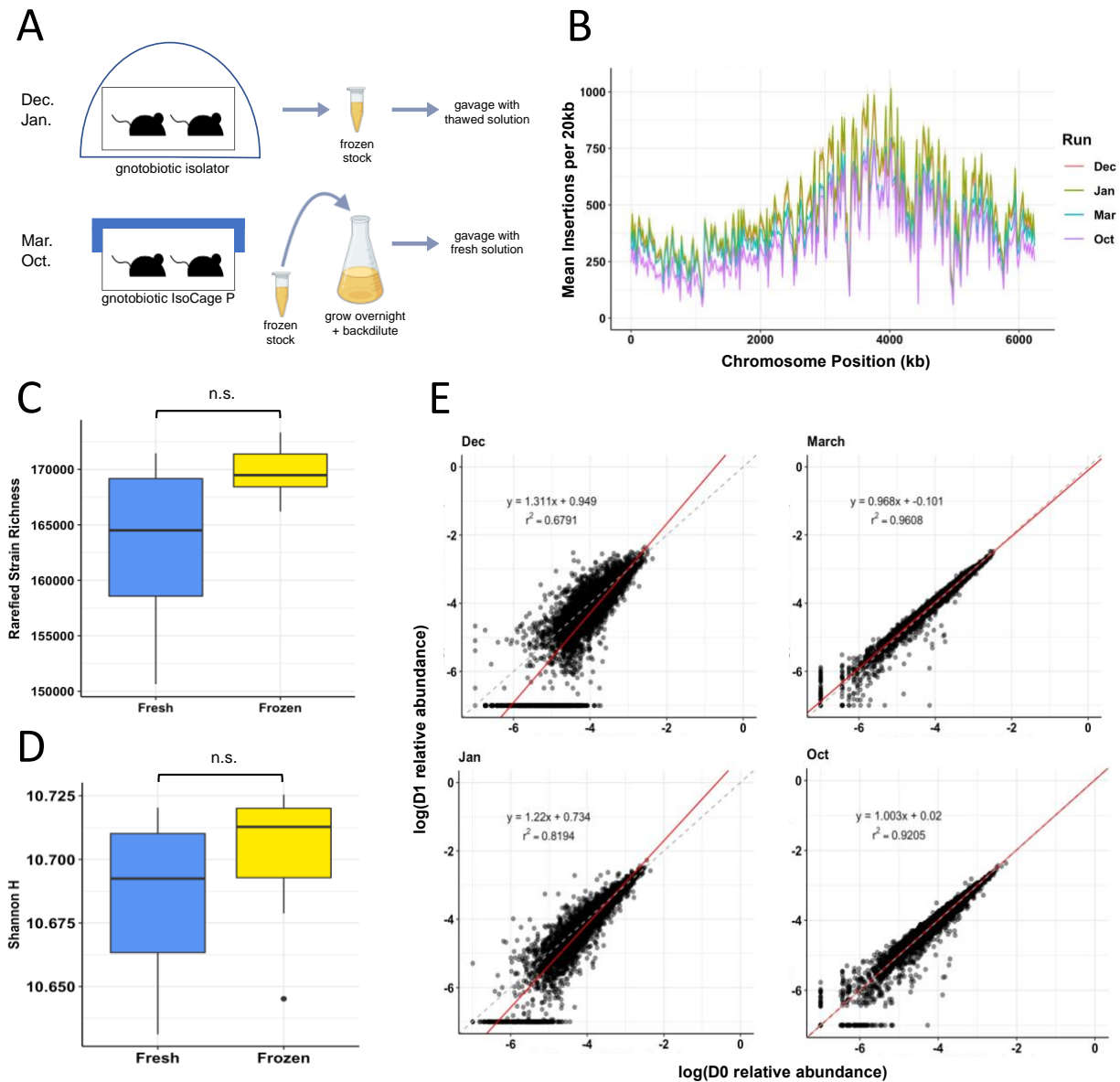


Fig. S1: Comparison of functional genetics experimental protocols and outcomes. A) Schematic representation of protocol differences across experimental cohorts. In Dec. and Jan. cohorts, mice were housed in cages of 2-3 animals within gnotobiotic isolators and gavaged with thawed stocks; in Mar. and Oct. cohorts, mice were housed in gnotobiotic cages of 2-3 animals on an IsoCage P Bioexclusion rack system and gavaged with stocks that had been grown overnight in fresh media. B) Mean number of unique mutant strains with RB-Tn insertions identified per 20kb region in inoculum samples from each experimental cohort. C) Rarefied strain richness is not significantly different across fresh and frozen inocula (two-sided Wilcoxon rank sum test, $p = 0.09$, $n = 8-13$ per group). Samples were rarefied due to uneven sequencing depth across experimental cohorts. D) Shannon diversity is not significantly different across fresh and frozen inocula (two-sided Wilcoxon rank sum test, $p = 0.1774$). E) Comparison of inoculum (D0) versus D1 relative abundance of each RB-Tn gene mutant. Dashed line represents 1:1, red line and equation represent linear regression best-fit line. Cohorts with frozen inoculum (Dec, Jan) experienced greater loss of mutants with low D0 relative abundance (< 0.0001) compared to cohorts with fresh inoculum (Mar, Oct).

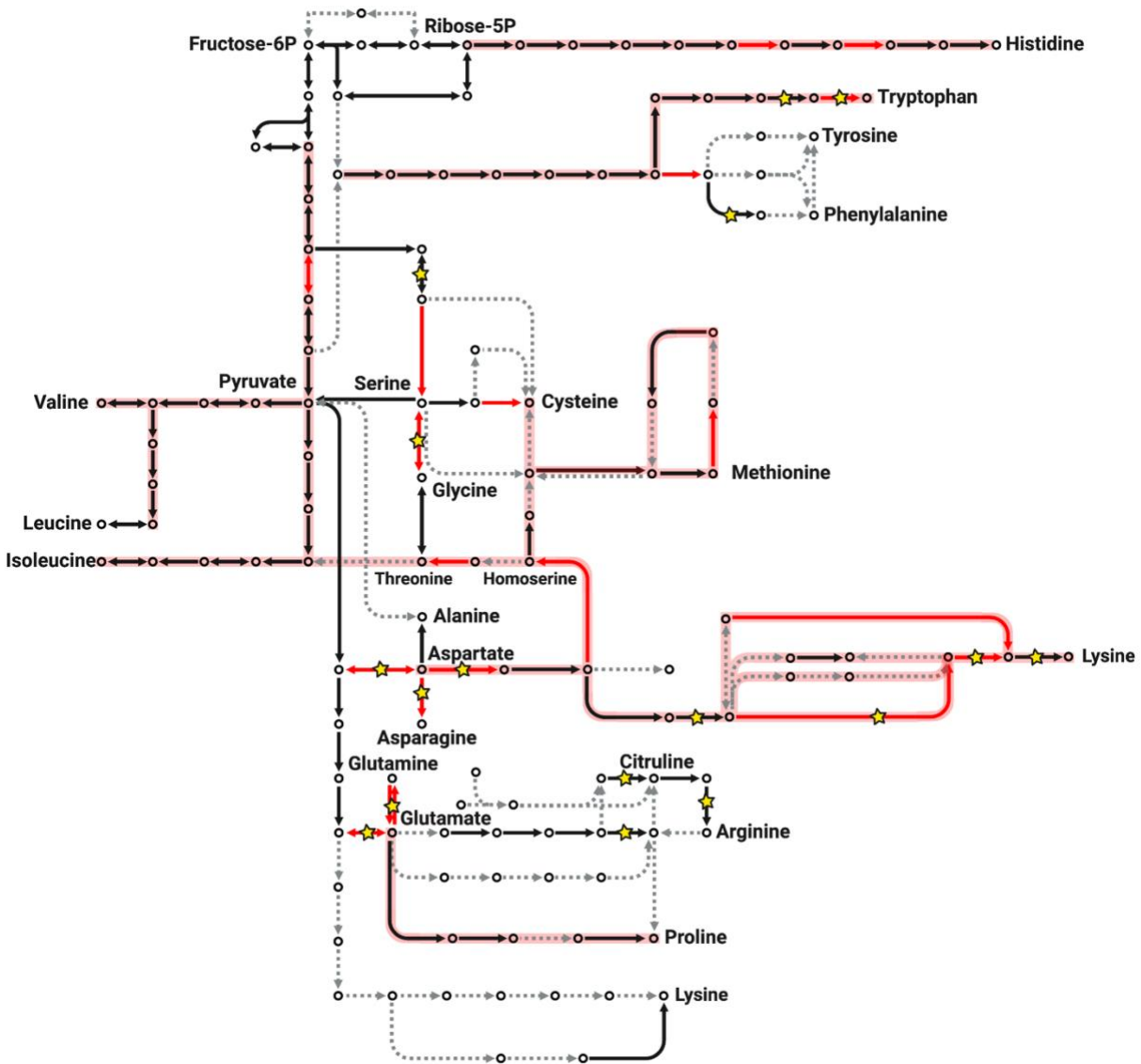


Fig. S2: Pathway map of reactions related to amino acid biosynthesis. Red arrows represent specific genes whose transcript is significantly enriched on D0.5/1 relative to D2/4 ($\log\text{FDR} < -3$, $|\log_2\text{FC}| > 2$, and base mean > 50 RPM), and red highlight represents pathways that were overall enriched on D0.5/1 relative to D2/4 ($\text{padj} < 0.05$). No genes or pathways on this map were relatively more expressed at D2/D4 than D0.5/D1. Genes whose transcript level did not differ significantly between D0.5/1 and D2/4 are colored in black. Grey dashed arrows represent reactions for which the associated gene is unknown in the *Bt* genome. Gold stars represent gene disruptions that were depleted in the RB-Tn assay, as in Fig. 2C. See also Table S6.

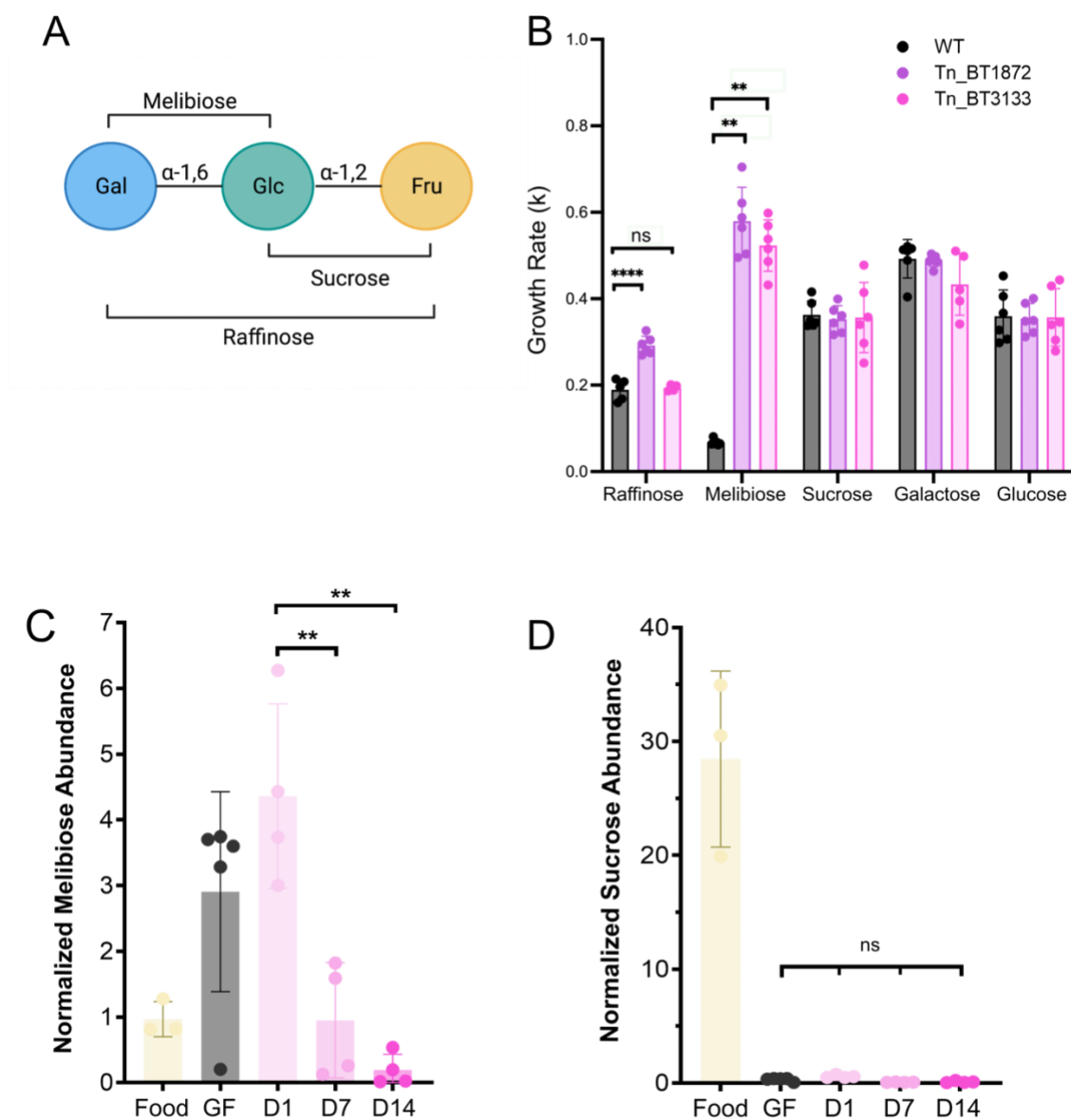


Fig. S3: *Bt* adapts to the GF gut specifically by increasing efficiency of metabolizing α -1,6 bonded sugars. A) Structure of the trisaccharide raffinose. B) The log phase doubling times of Tn_BT3133 and Tn_BT1872 were measured in Varel-Bryant medium with 20 mM raffinose, melibiose, sucrose, galactose, or glucose as the sole carbon substrate. Abundance of C) melibiose or D) sucrose in the standard chow fed to GF mice, within GF ceca before colonization, or 1, 7, or 14 days post-colonization.

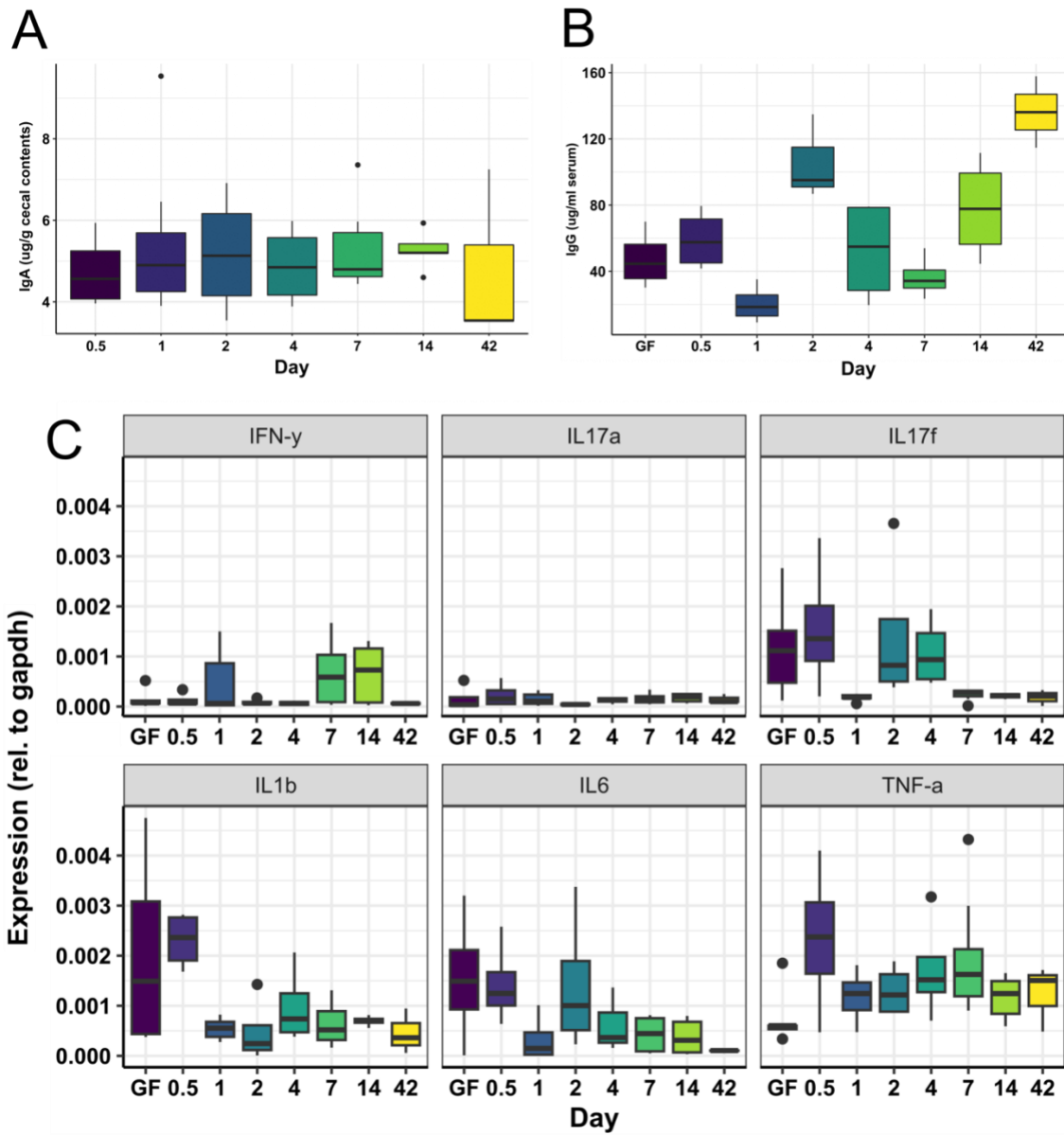


Fig. S4: *Bt* does not elicit a strong temporal host response. A) Cecal IgA and B) serum IgG levels from mice sacrificed at different timepoints after colonization (n=3-4/timepoint). C) Cytokine expression relative to gapdh in colonic mucosal scrapings at different timepoints after colonization (n=4-6/timepoint).

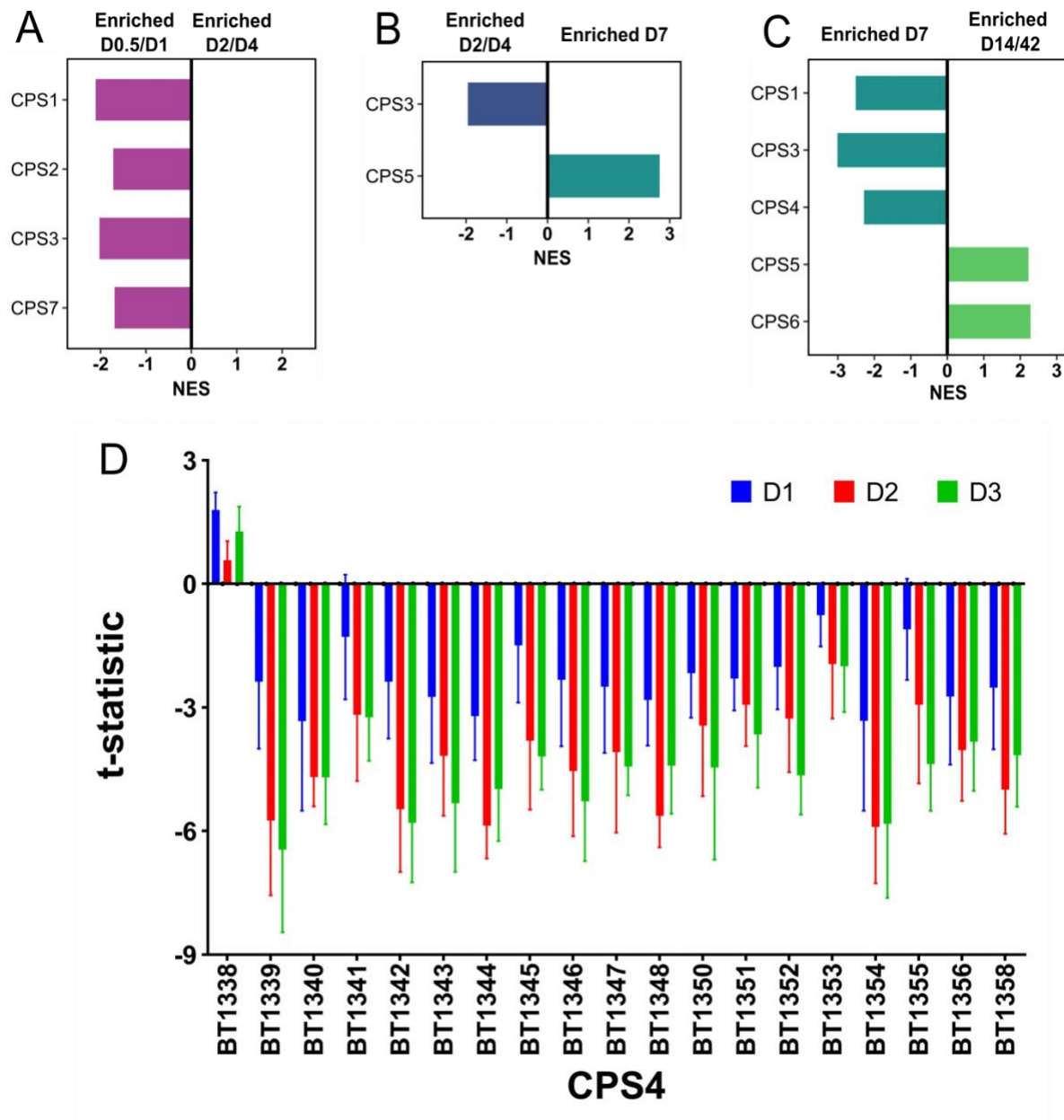


Fig. S5: Capsular polysaccharide biosynthesis operons are significantly associated with different stages of colonization. (A – D) Gene set enrichment analysis (GSEA) using transcriptomics data for capsular polysaccharide biosynthesis operons, comparing sequential timepoints. Only statistically significant (adj. $p < 0.05$) scores are shown. (E) Measurement of the adjusted t-statistic (12) in the RB-Tn assay on all days where fitness score was measurable (D1-3) shows that gene insertions in CPS4 consistently result in significant declines in mutant fitness for all genes within the CPS4 locus except for BT1338. See also Table S5.